UHASSELT
KNOWLEDGE IN ACTION

Maastricht University

Faculteit Geneeskunde en Levenswetenschappen
School voor Levenswetenschappen

master in de biomedische wetenschappen

Masterthesis

Electrical impedance tomography integrated with microfluidics: a characterization study for cell/tissue behaviour

Youssef El Jerrari

Scriptie ingediend tot het behalen van de graad van master in de biomedische wetenschappen, afstudeerrichting bio-elektronica en nanotechnologie

PROMOTOR :

Prof. dr. ir. Ronald THOELEN

BEGELEIDER :

De heer Marijn LEMMENS

2017
2018

De transnationale Universiteit Limburg is een uniek samenwerkingsverband van twee universiteiten in twee landen: de Universiteit Hasselt en Maastricht University.

UHASSELT
KNOWLEDGE IN ACTION

www.uhasselt.be
Universiteit Hasselt
Campus Hasselt:
Martelarenlaan 42 | 3500 Hasselt
Campus Diepenbeek:
Agoralaan Gebouw D | 3590 Diepenbeek

UHASSELT
KNOWLEDGE IN ACTION

Maastricht University

Faculteit Geneeskunde en Levenswetenschappen

School voor Levenswetenschappen

master in de biomedische wetenschappen

Masterthesis

Electrical impedance tomography integrated with microfluidics: a characterization study for cell/tissue behaviour

Youssef El Jerrari

Scriptie ingediend tot het behalen van de graad van master in de biomedische wetenschappen, afstudeerrichting bio-elektronica en nanotechnologie

PROMOTOR :

Prof. dr. ir. Ronald THOELEN

BEGELEIDER :

De heer Marijn LEMMENS

Acknowledgements

In the name of Allah, the Most Gracious and the Most Merciful. All praises belong to Him for the strengths and His blessing in completing this thesis.

First of all, I would like to thank some special people who helped me during the internship to bring this thesis to a successful end. I would like to express sincere gratitude to my promotor, prof. ir. dr. Ronald Thoelen, for the unique opportunity to be a part of his BDE-group at IMO. Your comments, suggestions and supervision have undoubtedly helped me through the whole work process. It was a nice experience to be involved in creating and building up creative things that are needed for the project or for the thesis. Furthermore, I would also thank my second examiner, prof. dr. Anitha Ethirajan, for her interest in my project.

Also special thanks to my daily supervisor, Marijn Lemmens. Your suggestions and comments were really important to have a good internship and thesis. It was not easy to explain the electronic domain and the program language MATLAB, but you managed to make everything clear to me. Beside of that, I would also thank you for in-between talks about the daily life. I wish you all the best and good luck in your career.

Furthermore, I want to thank all members of the BDE-group. Especially, Thijs Vandenryt , thank you a lot for the comments and suggestions during the coach meetings. You were ready for everyone's questions. Also a special thanks to all my (BEN) colleagues for the awesome two years that I have spent with them.

Of course, I would like to thank my family. Thank you, sisters and brothers, to be in my life. You had always encouraged me to work hard until the end. I would also like to thank my niece Yasmina for everything she did for my. Special thanks to the most important person, my mother Hassana. You did and gave me everything what I want. You taught me to never give up and to always believe that everything will be okay at the end. I felt your love everywhere and at every moment. Furthermore, I will not forget to thank Houda. Thank you both for your patience. Thank you so much to always be there for me.

My Idol, my father, who I lost when I was 11. It has been a long time without you. I know you are now in a better place and waiting for this moment. I would like to dedicate this thesis to you. Thank you, papa for your love, even though it was short, but I still feel it. I hope you are now proud of your son. You were great for the society as a head nurse in a small hospital. You are still remembered by everybody who met you. Thank you!

I will not forget to thank everybody who has consciously or unconsciously contributed to the realization of this thesis.

Youssef

Table of contents

Abstract

In the (bio)medical field of regenerative medicine, it is really important that we can assess structural responses of bodily tissues, guide them towards recovery and unravel the mysteries of regeneration. Therefore, a suitable technique for fast analysis is required. Electrical Impedance Tomography (EIT) is a promising method which allows a non-invasive, radiation free and inexpensive technique to characterize the dielectric properties of biological tissues and cells. The applicability of EIT in biomedical research has been acquired in different situations such as monitoring of lung ventilation, breast cancer imaging and brain imaging. In this thesis, a step towards a new system is taken to image the cellular growth, based on self-developed EIT sensor.

16 electrodes miniaturized EIT sensor with a customized readout device (Agilent 4284A) has been developed, that has the ability to image cells in 2D. The sensor was integrated in a flow cell, made of plexi glass to create culture chamber. This setup enables a fast and accurate analysis (differentiation) of cells and other micron sized particles based on impedance measurements. First tests were focused on the confirmation of the setup. Next, yeast cells (*Saccharomyces Cerevisiae*) were used as proof-of-concept to image the cellular growth. The measurements were acquired in function of time and were post-processed into conductivity distribution images using a finite element model.

Experiments have indicated that EIT is a viable technique to study the characteristics of different objects with different contrasting in conductivity. Additionally, tomography images of the thorax and the bladder were comparable with CT-scan images, which indicates the working of our developed setup. Finally, the results have demonstrated that the system was able to image the cellular growth of yeast cells. The mean impedance values of the boundary measurements, within the sensor, increases during the cellular growth. A clear difference was noticeable in conductivity distribution of the reconstructed images during the growth.

In conclusion, preliminary results indicate that the developed system is an important technique to study cell culture in 2D images. However, this project took the first steps towards new imaging technique for studying cell behaviour and was especially focused on the development and the characterisation of the setup, further optimization is still required. Imaging the cell behaviour with EIT will provide fast and important insights into the interaction between drugs and biomaterials which would be significant and useful for diagnostic and clinical applications. Taking together, EIT promises to become a valuable tool in multimodal applications for imaging the cell behaviour (cell growth, migration and morphological changes) as response to the introduction of drugs or biomaterials.

KEYWORDS: Electrical Impedance Tomography (EIT), Cell imaging, Cell proliferation.

Nederlandse samenvatting

In het (bio)medische gebied van regeneratieve geneeskunde is het belangrijk dat men structurele reacties van lichaamsweefsels kan beoordelen, en deze naar de juiste herstelplaats kan brengen en moeilijkheden van regeneratie kan ontrafelen. Een geschikte techniek voor een snelle analyse is nodig. Hierbij is de Elektrische Impedantie Tomografie (EIT) een veelbelovend techniek om de diëlektrische eigenschappen van biologische weefsels en cellen op een niet-invasieve, stralingsvrije en goedkope beeldvorming te karakteriseren. In deze thesis is een nieuw systeem ontwikkeld om de celgroei van gistcellen te monitoren. Dit systeem is gebaseerd op een zelf ontwikkelde EIT-sensor.

Een geminiaturiseerde sensor met 16 elektrodes en een aangepast uitleesapparaat (Agilent 4284A) is ontwikkeld dat in staat is om gekweekte cellen in beeld te brengen. De sensor was geïntegreerd in een flow cel, vervaardigd uit plexiglas. Deze sensor maakt een snelle en nauwkeurige analyse (differentiatie) van cellen en andere microdeeltjes na impedantiemetingen. Verder waren de eerste testen op de validatie van de setup gericht. Vervolgens werden gistcellen (*Saccharomyces Cerevisiae*) als validatie gebruikt om de celgroei in beeld te brengen. EIT metingen werden verkregen in functie van tijd en deze gegevens werden in tomografische beelden nagewerkt met behulp van een eindige element methode.

Experimenten hebben aangetoond dat EIT een rendabele techniek is om de kenmerken van verschillende objecten met verschillende contrasterende conductiviteit te bestuderen. Verder komen de tomografische beelden van de thorax en de blaas overeen met de verwachte resultaten uit de CT-scan. Ten slotte, het gemiddelde impedantiewaarden van de metingen binnen de sensor nam toe wanneer gistcellen begonnen te groeien. Na het verwerken van de gegevens is er duidelijk een toename zichtbaar in de conductiviteit van de tomografische beelden omwille van cellulaire groei.

Als conclusie tonen voorlopige resultaten aan dat het ontwikkelde systeem en de verkleinde EIT-sensor een belangrijke techniek kunnen zijn voor het bestuderen van cellen in 2D tomografische beelden. Het project was gericht op de ontwikkeling en het karakteriseren van de setup, desondanks is verdere optimalisatie nog steeds nodig. Wanneer het celgedrag met EIT bestudeerd wordt, zal een snelle en belangrijke inzicht in de interactie tussen geneesmiddelen en biomaterialen verschaft worden. Het huidige systeem is betekenisvol en nuttig voor diagnostische en klinische toepassingen. Samengevat, EIT belooft een hulpmiddel te zijn voor het weergeven van de kinetiek in de celgroei, de migratie en de morfologieveranderingen in functie van tijd na het indienen van geneesmiddelen.

TREFWOORDEN: Elektrische impedantie tomografie (EIT), Cel beeldvorming, Cel proliferatie.

List of abbreviations

2D	Two-dimensional space
3D	Three-dimensional space
AC	Alternating Current
BDE	Biomedical Device Engineering
CT	X-ray computed tomography
E	Electrode
ECG	Electrocardiography
EIT	Electrical Impedance Tomography
FEM	Finite Element Model
HP	Hewlett Packard
Hz	Hertz
LCR	Inductance, capacitance and resistance
MRI	Magnetic Resonance Imaging
PCB	Printed Circuit Board
PDMS	Polydimethylsiloxane
RM	Regenerative Medicine
S. Cerevisiae	*Saccharomyces Cerevisiae (*budding yeast or brewer's yeast)

List of symbols

Z	*Bio impedance*
V	Electric Voltage
I	Electric Current
λ	Lambda
S	Siemens
Ω	Ohm
A	Ampere
V	Volt
F	Farad
Φ	Phi

I Introduction

1 General Background

Researchers in the field of regenerative medicine (RM) tend to provide new mechanisms to enhance the regeneration and the repair of lost or damaged tissues and organs. Tissue engineering applications contain interfaces between the cells and the biomaterials. They try to combine stem cells with biomaterials in a three-dimensional (3D) way, which can be used as a preclinical tissue model. Therefore, this will be a promising source for an early stage of new therapies. That gives hope for many patients with several disorders such as heart, brain or spinal cord disease because they cannot regenerate by themselves [2].

During last decades, a number of excellent synthetic biomaterials have been developed for RM [3]. Yet, monitoring and assessing results of the interaction between the biomaterials and human cells remains challenging. Therefore, a new method to observe the cell-biomaterial interaction or the cellular progress is needed, on one hand to select only the most promising materials for further research but also to eliminate the poor materials at an early stage of development.

Both the pharmaceutical and biological industries are using traditional imaging techniques such as histological and immunohistochemical staining. These tools are familiar and have been used widely to evaluate the cell responses against drugs. However, these techniques require preparation such as cell labeling and they can lead to interpret results wrongly [4].

Several studies have shown the relevance of electrical impedance tomography (EIT) in (bio)medical applications [5]. It is a powerful method that characterizes the electrical properties of a material under test and has attracted ample interest in the field of biomedical imaging due to its high-speed, cost-efficient, label-free and non-intrusive sensing ability. EIT has been applied in different situations such as monitoring of lung ventilation, biological cell growth (breast cancer imaging) and brain imaging [6,7]. EIT is a method that produces 2D or 3D images that represent the electrical conductivity distribution of the measured region or the sample under test. It is quite similar to other imaging tools like x-ray computed tomography (CT) or magnetic resonance imaging (MRI). With these tools, a radiation or magnetic field is sent through the sample and the obtained signals will be used to reconstruct an absolute image. However, with EIT an electric signal is sent and the resulting voltage is measured.

Biological cells consist of a conducting cytoplasm with nucleus covered by a thin insulating membrane. This structure is interesting when an alternating current (AC) electric field is applied, because the cell membrane behaves like capacitor: the lower the frequency, the higher the resistance and vice versa. This means that the size and the shape of the cell can be obtained by measuring the electrical properties at low frequencies. The high frequencies at their turn can be used for characterization of the internal properties, such as cytoplasmic resistance. This means that EIT is an interesting and promising technique to study cells [6].

However, the human system is very complex with a lot of interactions and connections between all the organs. The cells that are growing in 2D culture Petri dish provide a different growing environment

than cells that grow *in vivo*. Hereby, there is a lacking of cell-cell and cell-matrix interactions [7]. A solution therefore would be to mimic the organ function which can be done by making a chip based on human cells as a model. This system is called an *organ-on-chip* and presents a better model for the human body than an ordinary petri dish. It is a micro-engineered cell culture device that tries to mimic the cellular microenvironment found *in vivo* with high accuracy by recapitulating the physiological function. They are promising as a solution for drug testing and also for cancer treatments. They provide more predictive preclinical tools than the standard *in vitro* and *in vivo* models [8]. Such devices open entirely new possibilities for drug screening. However, they also present new challenges in terms of readouts of quantifiable parameters. Researcher try to extract as many information as needed, preferably real-time, from a small amount of cells, cultured in tiny and confined volumes [9]. A study of Hun et al. demonstrated how lungs can be mimicked in a very small chip for the first time. This chip consists out a thin, porous and flexible membrane. Lung epithelial and endothelial cells were cultured on that membrane [8].

A combination of EIT with *organ-on-chip* will accelerate research in pharmaceutical companies and research institutes to bring new drugs and therapies on the market. When drugs are tested *in vitro*, the cells do not react as they would do in the human body. These results bring some doubts sometimes about the results false cell response and thus also in false interpretation of the outcomes. Furthermore, *in vivo* animal testing is also not completely reliable, because their metabolism is different than human cells and above this it is also time-consuming and expensive. An *organ-on-chip* device integrated with microfluidic chambers and the use of the patients' own cells will be a good solution to culture any cell type in a 3D culture chamber. In this way, the cells will behave like they will react in the human body. By integrating microfluidic *organ-on-chips* with EIT, the tomography images will be reconstructed. This provides information about the cellular growth and behaviour which is interesting for treatment of several diseases such as monitoring cancer cells. Moreover, it is also possible to obtain information about the cell-biomaterial interactions. This can be useful for optimization of different kind of prostheses.

The aim of this study is to develop an innovative system for monitoring the cellular proliferation. In the first phase, a new readout device will be developed, which will consist out of an inductance, capacitance, and resistance (LCR) meter and a multiplexer. This system has the ability for switching between multiple channels, accurate voltage measurement and has also the capability to generate a current with a low noise floor. This will be used to measure the potential when a known alternating current (AC) is injected. Thus, the impedance will be measured with Ohm's law. Furthermore, an EIT sensor chip with 16 electrodes will be designed and integrated into a flow cell to create a culture chamber for cells. Using this system, measurements data during cell proliferation can be taken and tomography images can be reconstructed from the impedance measurements during the cell proliferation in that culture chamber. Yeast cells will be used to monitor the cell proliferation, due to the fact that they proliferate very fast, and are easy to work with. This is an initial phase study and will assist the researchers to understand the interaction between cells and biomaterials and to accelerate the production of new and useful biomaterials for repair of damaged or diseased organs and tissues.

2 The basic principles of EIT

Biological tissues are conductive due to the ion homeostasis [10]. Some tissues contain more ions, which are free to carry charges, than others and are therefore more conductive. For example, bone is a poor conductor whereas muscle is relatively good conductor, also a difference in conductivity has been proven between cancer cells and normal cells [11,12]. The conductivity value is expressed in Siemens per meter (S/m) and the resistivity is inversely proportional with the conductivity and is expressed in Ohm meter (Ωm).

In a medical context, EIT can be used as an imaging technique because of the difference in the conductivity of the different tissues in the body **(Table 1)** [13]. The first published electrical tomographic images were those of Brown et al. in 1983 [14]. For example, if a set of electrodes surround a region of interest, impedance measurements can be performed by applying currents and measuring voltages. These obtained data set can be used to reconstruct a tomography image. The spatial resolution is dependent on the number of the measured datapoints. Therefore, the number of electrodes is important and as a result the resolution of EIT is poor compared to other imaging techniques. If 8 electrodes are used, only 56 measurements can be measured. However, 16 electrodes will give 240 data points and as a result much better spatial resolution [15].

Table 1 Conductivity values for tissues and organs in the human chest at 100 kHz [12].

Tissue	Conductivity (mS/cm)
Bone	0.06
Cardiac Muscle	6.3 (longitudinal)
	2.3 (transversal)
Fat	0.36
Lungs	1.0 (expiration)
	0.4 (inspiration)
Blood	6.70

2.1 Theoretical working principle of EIT

The EIT reconstruction tool tries to find a solution for a nonlinear problem by reconstructing the conductivity map in a closed domain (Ω). This is done by measuring the surface potentials at the boundaries of the object under test when a constant current is applied [16]. It is a highly ill-posed problem in which a small amount of noise in the boundary data can lead to enormous errors in the resulting image. Two different parts of the mathematical theory of EIT algorithm exist: the 'forward' and the 'inverse' problem.

The forward solver tries to determine the boundary potentials data and this for a known current injection pattern. The inverse solver on the other hand calculates the conductivity distribution for which the boundary voltage difference becomes minimum. First, the voltage mismatch vector is calculated by comparing the measured voltage values and the calculated voltage values using the following **equation (1)**:

$$\Delta V = V_m - V_c \qquad (1)$$

Where V_m is the measured potential value at the boundary and V_c is the calculated one. After ΔV is obtained, the conductivity distribution is estimated by solving the following Gauss-Newton equation (2):

$$\sigma_{k+1} = \sigma_k + \left((J^T J + \lambda I)^{-1}(J^T(V_m - f) - \lambda I\sigma)\right)_k \quad (2)$$

This means that the inverse solver tries to find a solution for the conductivity distribution matrix ([σ]) when the current matrix ([C]) and the potential value matrix ([Φ]) are known. The result of this equation is the conductivity and is expressed in (*S/m*).

Most EIT setups inject the current and measure the voltages. Therefore, the conductivity, which is the unknown parameter, can be calculated using Ohm's law. The EIT algorithm works as follows: the boundary voltage values for a known current injection and an initial guess for the conductivity matrix. When the potential distribution matrix is found, the Jacobian is calculated. Gauss-Newton equation is then used to calculate the new conductivity vector. Next, the conductivity matrix is generated by adding the updated conductivity vector to previous conductivity result. The new conductivity matrix is used in the forward solver to find a new voltage mismatch vector. Finally, the voltage mismatch vector will be checked if it satisfies to the requirements of the specified threshold for the error margin. Hereby, an approach solution for the conductivity value matrix is found. Thus, the image can be created based on these conductivity values [17]. For a good resolution image, the number of electrodes should be high enough to obtain enough measurements data points to get a good image. On the one hand, the forward solver has to find a solution for the potential value matrix. On the other hand, the inverse process works in the opposite way. A more detailed information about the mathematical working of EIT algorithm is well described in the literature [16,17].

2.2 Four-points vs two-points measurements

During this internship, the developed system has the ability to measure the impedance using either two or four connections. Each measurement method has advantages and disadvantages. To make a conductivity distribution, 4-points measurements is preferred.

A 4-points measurement eliminates the contact impedances by using two electrodes as current injection electrodes and two electrodes are measuring the voltages. This configuration provides a more accurate impedance measurement than the 2-points configuration due to the absence of the parasitic resistance of the wires. It separates pairs of current carrying and voltage-sensing electrodes to make more accurate measurements. This separation of current and voltage electrodes eliminates the lead and contact resistance from the measurement.

A drawback of 4-point measurements *in vivo* is the "current path problem" because of the non-ideal contacts between the electrode and the tissue sample in inhomogeneous materials. The current will go directly to homogeneous materials, while in non-homogeneous materials the current will take the path of least resistance. Yet, the current path problem is worse in a 4-point measurement. The measurement of impedance using a collinear arrangement of 4 electrodes depends on the hypothesis

that current driven between an outer pair of electrodes passes through the material uniformly, and thus the voltage measured by the inner sense electrodes can be used to calculate impedance from Ohm's law. When the current takes an unknown path between the drive electrodes instead of passing straight through the materials below the sense electrodes, the actual voltage generates using **equation (3)**, whereby V the potential, Z is measured impedance and I is the current [18].

$$V = I * Z \tag{3}$$

2.3 Applications of EIT

EIT has a lot of advantages, such as high temporal resolution, inexpensive, non-invasive and non-radiation. The use of EIT as a routine clinical tool had known slow progression over time. However, EIT is most likely a competitive medical anatomical imaging techniques compared with CT and MRI. Nevertheless, applications of EIT span over a wide range of fields to solve many problems in (bio)medical application.

EIT has been used for tomographic imaging in the medical field to visualize the anatomy and the physiology of the human body. For instance, the rate of gastric emptying can be monitored using EIT [19]. Also, a cross-sectional image of the changes in resistivity distribution within the chest can be produced to monitor lung ventilation. EIT can also make a difference in the field of neurology, by which during cerebral ischemia, the impedance of the brain tissue increases and thus allows for a non-invasive method for assessing brain strokes [19]. Furthermore, material engineering and semiconductor manufacturing are studied using EIT technique to estimate the thickness of the polysilicon film by measuring the conductivity distribution. In biotechnology, cell growth was monitored using EIT [5,20]. In addition, EIT has also shown promising results in geophysics such as oil exploration [21]. To conclude, EIT can be performed in different areas, for different purposes and needs to be proved for using it in the clinical field.

3 Comparison of EIT with other tomography imaging methods

In the (bio)medical field, a limited number of imaging techniques is familiar which are known for their sensitivity and accuracy. However, the used techniques such as MRI, CT scan and positron emission tomography (PET) show some drawbacks.

In order to image the nerves and the muscles is MRI the most suitable technique. It uses magnets (0.5 - 7 Tesla magnetic field strength) to polarize the hydrogen nuclei in water molecules in human tissues. Dependent of the time-varying gradient, magnetic fields and the pulse sequences of radio frequency waves, the spatial distribution of signals emitted from protons is provided. Luckily, no ionizing radiation is used. It is one of the most versatile clinical imaging tools, with his superior sensitivity in imaging the morphology and pathology [2].

Furthermore, the classical CT scan uses computers-processes X-rays to reconstruct tomographic images. This technique has been used to image the bone fractures and also tumours. The drawback of this technique is the use of ionizing radiation, which can damage the DNA. Next to this, PET is a tomography technique that produces images of functional processes in the body through detection

of biologically active positron-emitting radio-tracer attached to a small molecule. This technique is very sensitive and has no limit on tissue penetration. These conventional tomography techniques are expensive, requires large hospital spaces, and are not safe for the human body because of the radiation [2].

All these imaging techniques try to produce an accurate image of the internal structure. EIT does this by using an electrical field to derive the conductivity distribution, whereas CT and MRI use radiation and magnetic fields respectively. EIT can be an attractive alternative and an important competitive technique for these techniques. Moreover, EIT uses the low current and does not cause any long-term harm to the body. One of the major drawbacks of EIT is the low spatial resolution since it depends on the number of the electrodes. It has potential to be a conventional imaging tool in medicine and research because of that its non-invasive, inexpensive and easy to use character [2].

4 Biological tissues and electrical properties of cells

When electronic technology integrates with medical technology, new biomedical devices can be developed which are able to diagnose some diseases. Several studies have reported that cellular detection can be monitored by means of its biological electrical impedance (BioZ), both *in vivo* and *in vitro* experiments. Bio-impedance, denoted by "Z", is one of the major electrical properties of flow biological tissues.

The cellular sample suspensions can be described as a network of electrical passive components. The simplest model of a cell consists of a single resistor and capacitor in series with each other, representing the cytoplasm and plasma membrane respectively. The resistance is due to the flow of ions among the cells and is related by Ohm's law to current. The capacitance is a measurement for the amount of electric charge stored on both sides of the membrane that can be defined in the form of the electrical potential. A biological cell exists of charged proteins in the cytoplasm covered by a double lipid layer that separates ions from the extracellular space. The pure lipid membranes are excellent electrical insulators, but a real cell membrane consist of a dense mosaic of proteins and lipids. These proteins act as channels and allow charges to pass. They play an important role in the electrophysiology of the cell and reduce the high resistance of the membrane. The cell membrane can be described as a simple group of electronic components (Randles cell), the extracellular space is represented by a resistor (R_e) and the intracellular space and the cell membrane are represented by a resistor (R_i) and a capacitor (C_i) **(Figure 1)** [22]. Both membrane resistance (R_m) and the membrane capacitance (C_m) occur over the cell membrane which is electrically parallel. Therefore, the cell membrane acts as a filter on current or voltage injected into the cell [23].

When an alternating current (AC) electric field is applied, the cell membrane behaves as an insulator at low frequencies and as a conductor at high frequencies. As shown in **figure 2**, when high-frequency measurements are applied, the current passes right through the membrane. In this situation, the plasma membrane acts as a short and the cell acts as a resistor, thus allowing the electrical properties of the cytoplasm to be probed. The result is dependent on the tissue and the liquids inside and outside the cells. While at low frequencies, the membranes impede the current flow. Therefore, bio-impedance can be used to measure volumes, shapes or electrical properties of biological cells. In EIT, cells can be placed between multiple electrodes. When the cells proliferate, the impedance will change and thus images can be generated from the conductivity distribution [6].

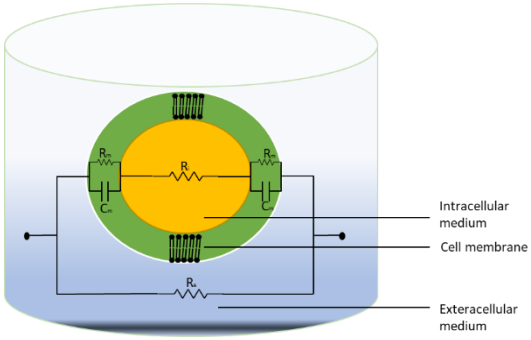

Figure 1 Cellular electrical model. *The membrane acts as a capacitor C_m and as resistor R_m, the cytosol as a resistor R_i and the medium as resistor R_e.*

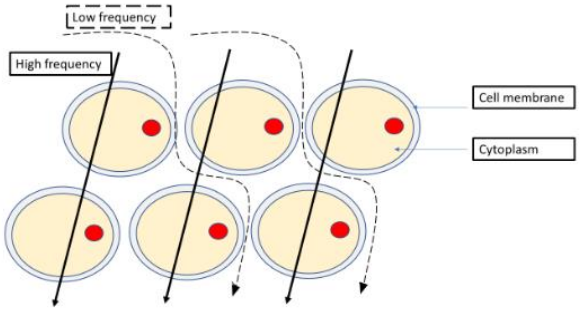

Figure 2 Impedance properties of tissues*. At high frequency, the current flows through the membranes. At low frequency, the current flows between the cells, because it cannot pass the membranes.*

The great advantage of using impedance measurements in cell studies is that labeling is not needed for detecting cell viability. Therefore, EIT enables to test the cell responses on non-invasive way. Furthermore, there is a large resistivity contrast between a wide range of tissue types in the body. Therefore, and it is thus possible to use resistivity to reconstruct anatomical images of the interest region. Moreover, in most cases, there is a significant contrast between normal and pathological tissue in conductivity and can be imaged and investigated using EIT [11].

II Materials and methods

1 System instrumentation

Two different setups were used for the impedance measurements: the MUSEIC V2.0 and the Agilent 4284A Precision LCR Meter. The MUSEIC V2.0 setup can only switch between 8 electrodes (Measurements International, Ontario, Canada). This low power multi-sensor acquisition system was developed by the researchers at IMEC (Leuven, Belgium). The currents were ranged from 10 µA to 100 µA and the frequency from 1 kHz to 8 kHz [24]. Schematic representation of the MUSEIC device is shown in **figure 3**.

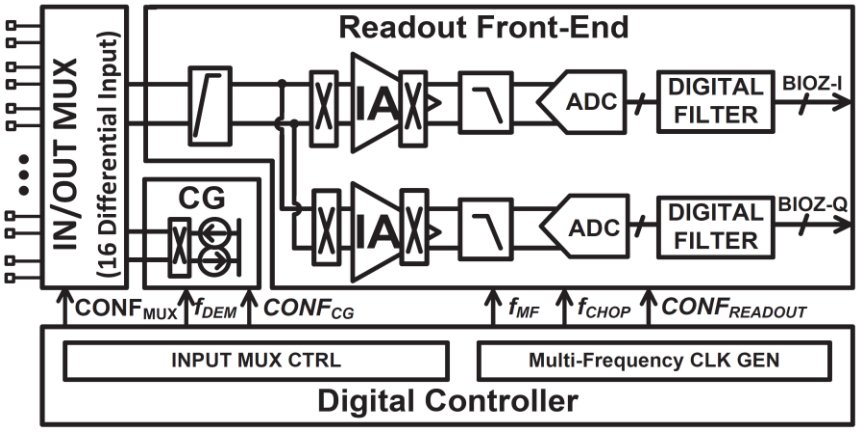

Figure 3 A schematic representation MUSIECV2.0*. IMEC (Leuven)*

On the other hand, for the measurements with 16 electrodes, the Agilent 4282A Precision LCR Meter (Agilent, Ca, USA) was used. The LCR Meter was controlled by a GPIB-GPIB interface with the PC. A multiplexer (Keithley) is used to switch between the channels through a self-made printed circuit board (PCB). Two multiplexer cards were used to control the switching. The first one supplies excitation to the electrodes and the second one acquires the measurements. Each multiplexer card contains four flat-cables and each flat cable consists out of 16 wires. Thus, 64 cables were joined together on the PCB. From this PCB, 16 outputs are used to make the measurement of the test object to perform frequency sweeps and to record the impedances. A software written in LabVIEW is used to control both the Precision LCR Meter and the multiplexer hardware. Different parameters, such as frequency, current and number of repeats, could be controlled by the parallel port of the PC.

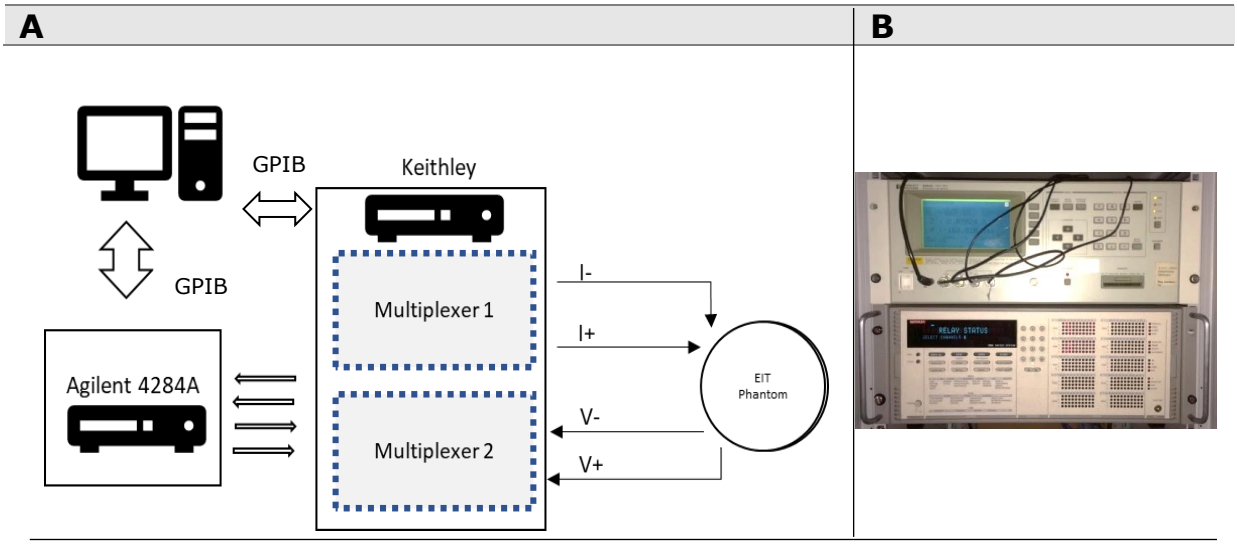

Figure 4 A: A simple representation of the block diagram of the new EIT hardware setup for 16 electrodes measurements. B: A picture of LRC meter *[Hewlett Packard (HP) 4284A and the multiplexer]*

Since different measurement patterns exist for EIT, different configurations are needed for the desired measurement method. The desired configuration can be loaded (Excel-CSV-file) in LabView. Hereby, a suitable switching pattern for the multiplexer is installed. The multiplexer enables excitation sequence of the current injection and the voltage measurement pattern to be applied onto the sensor electrodes. The used setups devices, Agilent and MuseicV2.0 have different parameters of measuring **(Table 2)**.

The data acquisition system collects differential voltage values from the interested material and converts them into digital output values and transfers the data to the PC. The received data is saved as a TXT-*file*. This data is processed by using MATLAB to produce tomography images using image reconstruction algorithms. This reconstruction is described in bit more in detail next.

Table 2 Parameters of the two setup devices.

	MUSEIC V2.0	***Hewlett Packard (HP) (Agilent 4284A)***
Measurement technique	Single-ended / differential	Single-ended / differential
Frequency range	20 - 40 kHz 1 kHz – 1 MHz	20 Hz – 1 MHz
Communication	USB	GPIB
Measurement electrodes	Two/four-point measurement	Two/four-point measurement
Channels	8	16
Current range	5µA – 100 µA	50 µA-20 mA
ADC precision	12-bit Multi-frequency 18-bit fixed frequency	11 bit

2 Measurements patterns

There are different ways to measure the boundary potential values. Moreover, the current injection can also be applied in various ways. In this thesis, the most common methods, the adjacent and the back-projection were used. Both methods are performed with 8 electrodes (E1, E2, …, E8) and with 16 electrodes (E1, E2, …, E16).

The adjacent method, also known as the neighbouring method, uses 4-points measurements whereby the current is injected in two neighbouring electrodes and the voltage is measured in other following neighbouring electrode pairs. When measurements with 16 electrodes were performed, the following scheme was followed: in the first cycle of measurements, the current is injected in E1-E2 and the voltage is measured in the electrode pairs E3-E4, E4-E5, …, E15-E16 **(Figure 5A)**. Note that electrode-pair E1-E2, E2-E3, and E16-E1 are excluded from the voltage measurements. The next cycle of measurement is equal to the first cycle unless the current injection is now on E2-E3 and the voltage measurements are now E4-E5, …, E16-E1. After 16 cycles of measurements, 208 data points are obtained **(Table 3)**.

On the other hand, the back-projection method, 2-points measurement, measures the voltage at the same electrodes where the current is injected. The first measurement is when the current is injected in E1-E2 and the voltage is measured in E1-E2. For the second measurement, the first electrode is taken as a reference electrode and the current is injected in E1-E3 and the voltage is measured in the same electrodes E1-E3 **(Figure 5B)**. The end of the first cycle would be thus E1-E16 where the current is injected and where the voltage is measured [25].

Table 3 Shows the number of the data measurements obtained from different methods.

Method	**8 electrodes**	**16 electrodes**
Adjacent	8 x 5 = 40 Data points	16 x 13 = 208 Data points
Back-projection	8 x 7 = 56 Data points	16 x 15 = 240 Data points

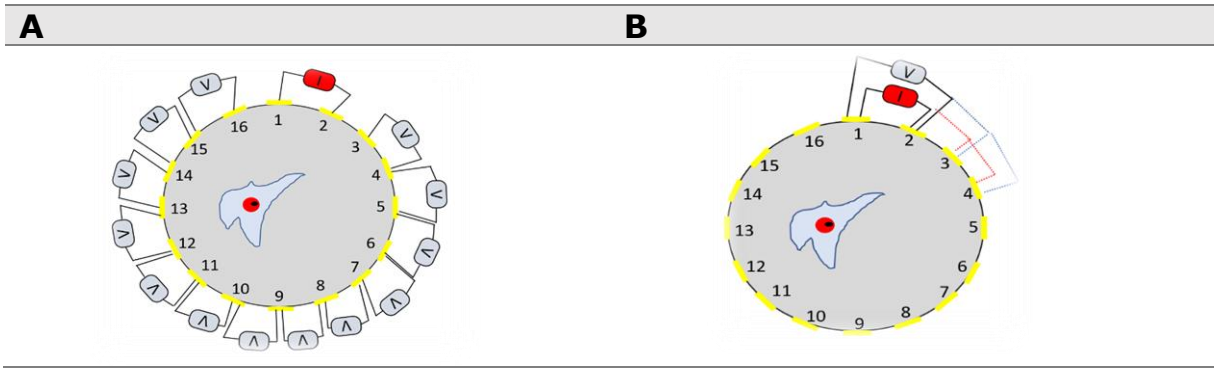

Figure 5 Schematic drawing of the two used methods. A: *The adjacent method, the current is injected in E1-E2 and the voltages are measured in the neighbouring electrode clockwise (E3-E4, …, E15-E16).* ***B:*** *The back-projection method, the current is injected in E1-E2 and the voltages are measured in the same electrodes*

3 Linear measurements

As a proof-of-concept for linear measurements, sixteen silver electrodes were printed in a plastic paper using a printer (Epson ET-3500). A squared container (8 cm x 2 cm) was attached to the paper where the electrodes located by using 2-compound epoxy. A conductive object was placed in different positions (left, middle, right) and measurements were performed using different methods namely, the adjacent and the Wenner method [26]. The tomography images were reconstructed using MATLAB (MathWorks, Inc., USA) [1]. **Figure 6** shows an image of the test setup for the linear measurement [21].

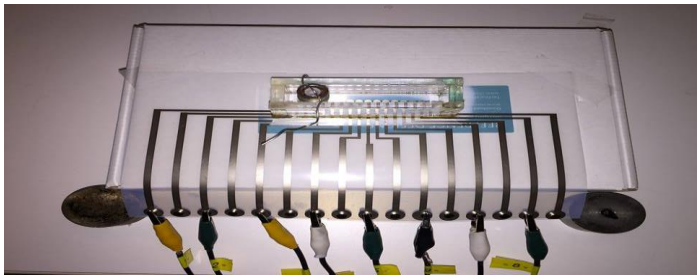

Figure 6 A picture of a proof-of-concept setup for the linear measurement. *A conductive object as seen in the picture was placed in different places.*

4 Image reconstruction

In this section, EIT reconstruction technique will be discussed in general. The tomography images were reconstructed using Electrical Impedance Tomography and Diffuse Optical Tomography Reconstruction Software (EIDORS). This is an open-source software toolbox for MATLAB. When the data of the measurement are collected, they will be loaded in MATLAB to reconstruct the tomography images. In order to obtain a good image, different solvers and filters should be chosen during the image reconstruction.

The most important one is the choice of the hyperparameter (λ) or the regularisation parameter. This parameter chooses a ratio between the image resolution and the smoothing of the data. It is used to convert the ill-posed problem into a well-posed problem using a suitable regularization parameter. It improves the reconstructed image quality. There are different methods to select the hyperparameter: The fixed noise figure, (SNR), the L-curve and the Generalized Cross Validation method.

The second selection that should be done is the Prior selection. These image priors are powerful to improve the quality of the reconstructed imaged. The most used priors are: Laplace prior, Tikhonov and Newton One Step Error Reconstructor (NOSER). Laplace prior was used for the measurements in this thesis. This prior gave a good result during the bachelor thesis of my colleague. Combining all of those possibilities to find the optimal solution **(Figure 7)** [17].

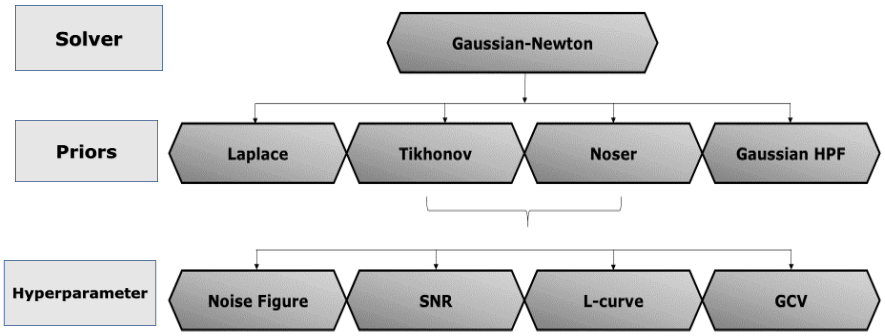

Figure 7 The combination algorithm for reconstruction tomography image. (The first row): *The solver is an iterative approach to determine the conductivity distribution of the reconstruction model.* ***(The second row):*** *The prior filters which are spatial filters applied to the data for a smoother conversion towards the conductivity matrix.* ***(The third row):*** *The hyperparameter algorithm to determine the hyperparameter, which is a regularization parameter that helps to solve the ill-posed problem.*

Two different types of images can be reconstructed: differential and static images. In differential images the reconstructed image is computed by subtracting one data set from the background data set, this results in a more accurate image. Furthermore, this includes the exclusion of the contact impedance and errors in the electrode position. On the other hand, a static image is constructed on the basis of one data set. This technique is interesting when the changes in the measured voltages is large between two data sets. It is difficult to find the optimal solution for image reconstruction if the measured voltages are too small. In this thesis, the used parameters for each reconstructed EIT images are summarized in a table that can be found in the appendix **(table S1).**

5 Chip fabrication

An EIT chip sensor with gold-plated electrodes was used. Firstly, the electrodes were schematically drawn using the CAD software. The chip design consists out of 16 electrodes positioned in a circular pattern as shown in **figure 8**. Two different designs with different diameters were performed: 2 mm and 6 mm. A silkscreen layer was used to isolate the leads from the electrodes to the pads. The electrode length and spacing are identical: the electrodes are 200 µm wide 235µm long.

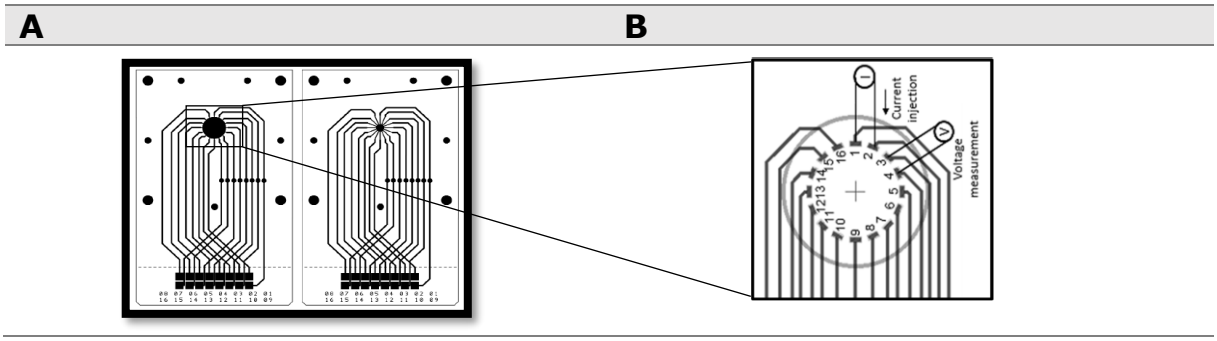

Figure 8 The path of the 16 gold electrodes from the sensor to the headers. A: *A schematic of the EIT sensor.* ***B:*** *A zoom-in on the circular part of the sensor.*

6 Closed flow cell / culture chamber for yeast cells

In order to measure the yeast growth, a flow cell was used and was integrated with the fabricated EIT chip. This flow cell was made out of two pieces of plexiglass and has a culture chamber, where the cells can proliferate. The flow cell has an input and an output channel to provide the cells with nutrients. The EIT chip sensor was put between the plexiglasses. A Polydimethylsiloxane (PDMS) O-ring was used to avoid any fluid leak **(Figure 9).** For most measurements, two sensor were running in a culture over, one sensor was connected to Agilent and the other one to MUSEICV2.0 **(Figure 10)**.

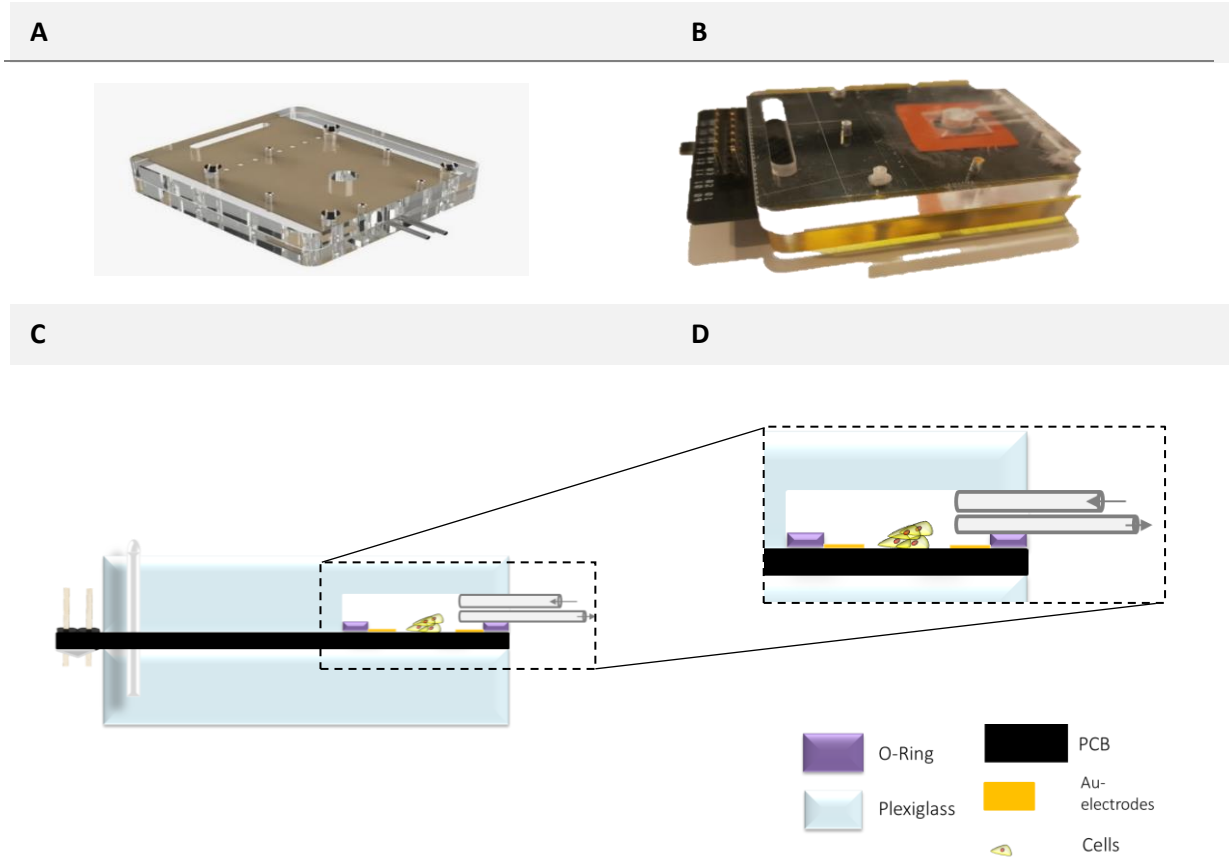

Figure 9 An overview of the flow cell. A: *A 3D design of the flow cell.* ***B:*** *A picture of the EIT chip integrated in the flow cell and a culture chamber is obtained.* ***C:*** *A cross-section of the flow cell with EIT chip.*

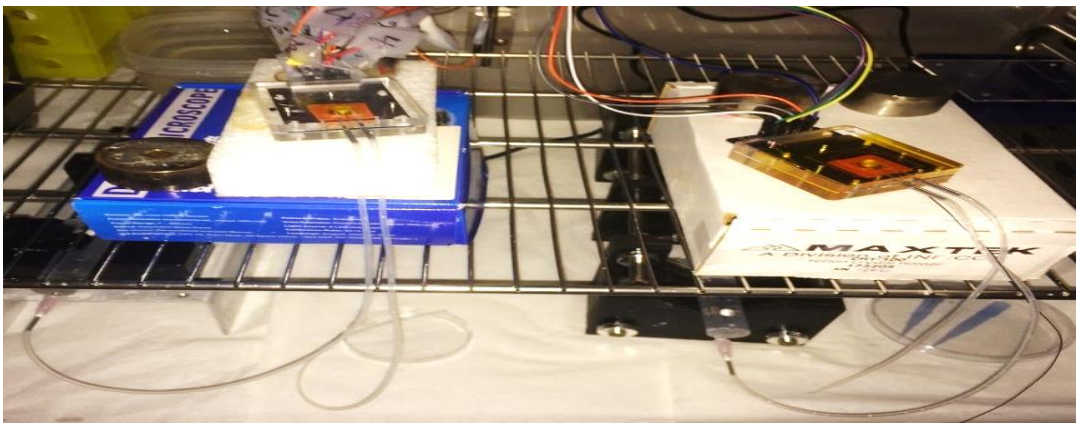

Figure 10 The whole setup in a culture oven*: Two flow cells are running, one was connected with 16 electrodes and controlled by Agilent 4284A and the other one was controlled by MUSEIC 2.0V and only 8-electrodes were used.*

III Results and discussion

The results of the EIT measurements will be discussed in the following subchapters. In order to evaluate the performance of our EIT system, different tests have been carried out for validation. The characteristics of the connections were tested using a Randles circuit as a reference. Next, the EIT system was tested using silica beads (Si-beads), which are less conductive. Due to this property, the EIT system is able to detect them in the developed miniaturized sensor. On the other hand, electrically conductive silicone, which are more conductive, are also used to test the homogeneity distribution of these particles. Additionally, tomography images of human tissues, such as the thorax and the bladder, were performed. These results are described in the appendix. Finally, the new miniaturized EIT sensor, integrated in a flow cell, has been used to monitor and to study cell proliferation using yeast cells as proof-of-concept.

1 Characteristics of EIT setup

The characteristics of the setup for the measurements, coming from the multiplexer to the EIT sensor, were tested using a simple three-element Randles cell model electrode-electrolyte model consisting of a charge solution resistance (R_1), a double layer capacitance (C) and a charge transfer resistance (R_2). On these elements, the connections and the settings were evaluated. The equivalent circuit of the Randles circuit is illustrated in **Figure 11**.

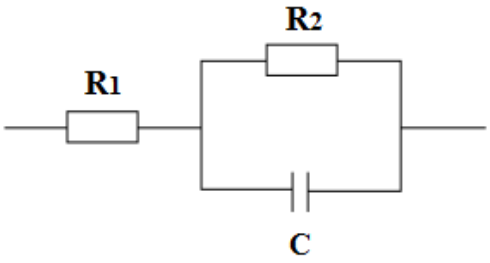

Figure 11 Equivalent of the reference Randles cell *R_1 = 10 kΩ, R_2 = 100 kΩ and C =1 nF.*

All connections of the cables were evaluated by measuring the impedance between two electrodes (E1-E9, E2-E10, …, E8-E16) by applying a current of 1 mA through the cell. Each measurement was repeated 10 times. By fitting the obtained data in function of frequency, an overlap of all frequency spectra is observed **(Figure 12)**. Furthermore, the graph goes from a magnitude of 110 kΩ to 10 kΩ, which indicated that the signal at low frequencies goes over R_1 and R_2, while the capacitor behaves as an insulator. On the other hand, at high frequencies, the capacitance becomes as a short circuit and the signal passes only R_1 and through C, which gives only 10 kΩ. Here, the current goes only through R_1 (10 kΩ). Also, the standard deviation was calculated and it was so small that it was not noticeable in the graph. All these results indicate that noise in the setup is limited.

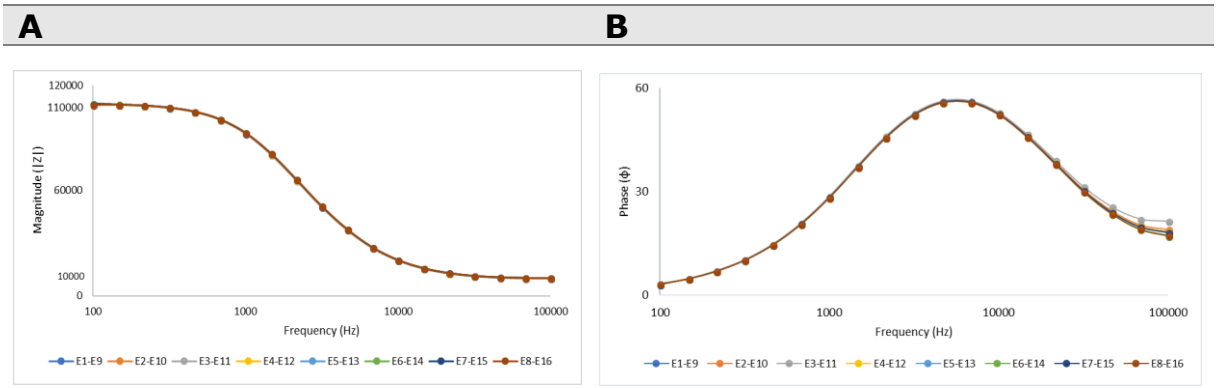

***Figure 12 A bode plot of the connections**. The magnitude and phase of the Randles cell between all electrodes.*

After evaluating the hardware, the characteristics of the EIT sensors were tested. For this, the cell constant was calculated for both EIT sensors with different diameter (2 mm and 6 mm). This is the ratio of the distance between the electrodes to the area of the electrodes **(equation 4)**. This value is calculated for recalculating the conductivity values from the reconstructed images.

$$K = \frac{d}{a} \tag{4}$$

Whereby: K is the cell constant (cm^{-1}), a is the effective area of the electrodes (cm^2) and d is the distance between the electrodes (cm).

One of the parameters which should be determined during the image reconstruction is the background value. This should be as close as possible to the conductivity value of the medium that is used. This value can be calculated using the following equation:

$$\kappa = G * K \tag{5}$$

where κ stands for the conductivity (S/cm), G is the conductance (S) ($G = \frac{1}{R}$) and K is the cell constant (cm^{-1}).

Table 4 Shows the cell constant of both sensors with different diameters.

	Distance between electrodes (cm)	**Area of the electrodes (cm^2)**	**Cell constant (cm^{-1})**
Sensor 1 (⌀ 6 mm)	0.53	0.00063	844.4
Sensor 2 (⌀ 2 mm)	0.19	0.00026	1146

1.1 EIT of silica beads

In this section, the EIT sensor was tested using Si-beads. This experiment was performed as a proof-of-concept for the EIT sensor due to their high resistivity compared to the saline solution (0.9 % NaCl). The particles were in the range of 70 - 200 µm (LC 60A purchased from Davisil).

The measurements were performed twice using the adjacent method. The first experiment was performed only on saline solution and was used as a reference. The next measurement was performed after adding Si-beads to the saline solution. A significant difference was noticed on the raw data **(figure 13)**. The saline solution with Si-beads shows a higher resistivity than the saline solution alone, as expected. The measurements were taken at different frequencies within the range of 1 kHz- 10 kHz. At high frequencies, the current will go through the solution and that the particles will not be observed in tomography images. The reconstructed images from this data are illustrated in **figure 14**.

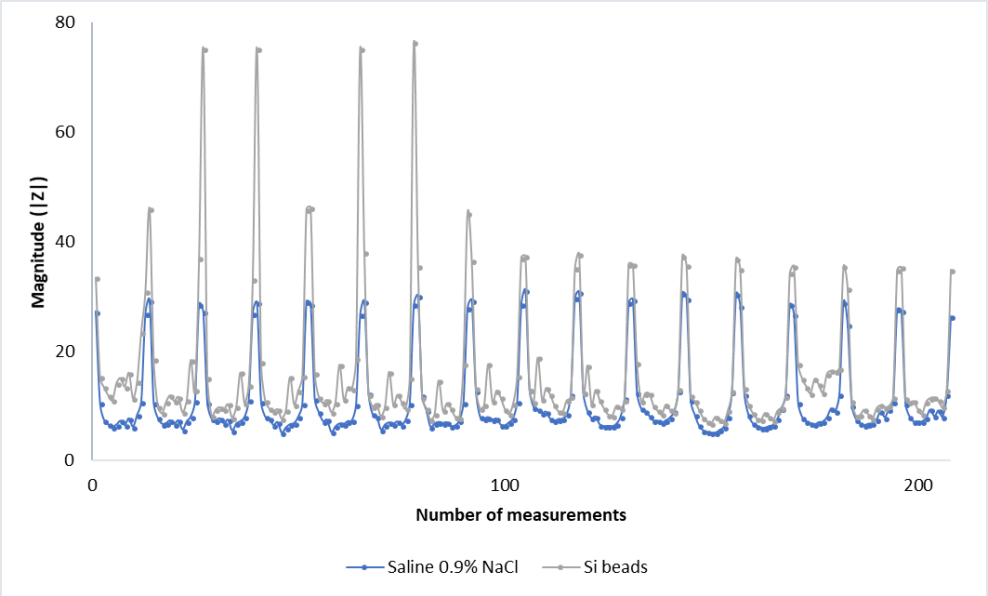

Figure 13 Raw data of the measured magnitude of Saline (0.9 % NaCl) and Silica beads. *The measurements were taken at a frequency of 1 kHz.*

The effect of Si-beads can be noticed at lower frequencies. Hereby, the tomography image is bluer than the background, which means that the conductivity distribution of the sensor is decreased after adding Si-beads. On the other hand, at high frequencies, the tomography images of Si-beads are comparable with those of the saline solution, which indicates that the current path went through the solution and the particles could not be observed. Note that the values of the colour bar of the images are normalized between 0-1, which means that the red region is more conductive and the blue is less conductive. When data of the saline solution alone (background) is subtracted from data of the saline solution with Si-beads, Si-beads are than observed in the reconstructed images. Hereby, the Si-beads are clearly visible **(Figure 15)**. That means that the most optimal differential images are obtained due to the small changes in the measured voltages.

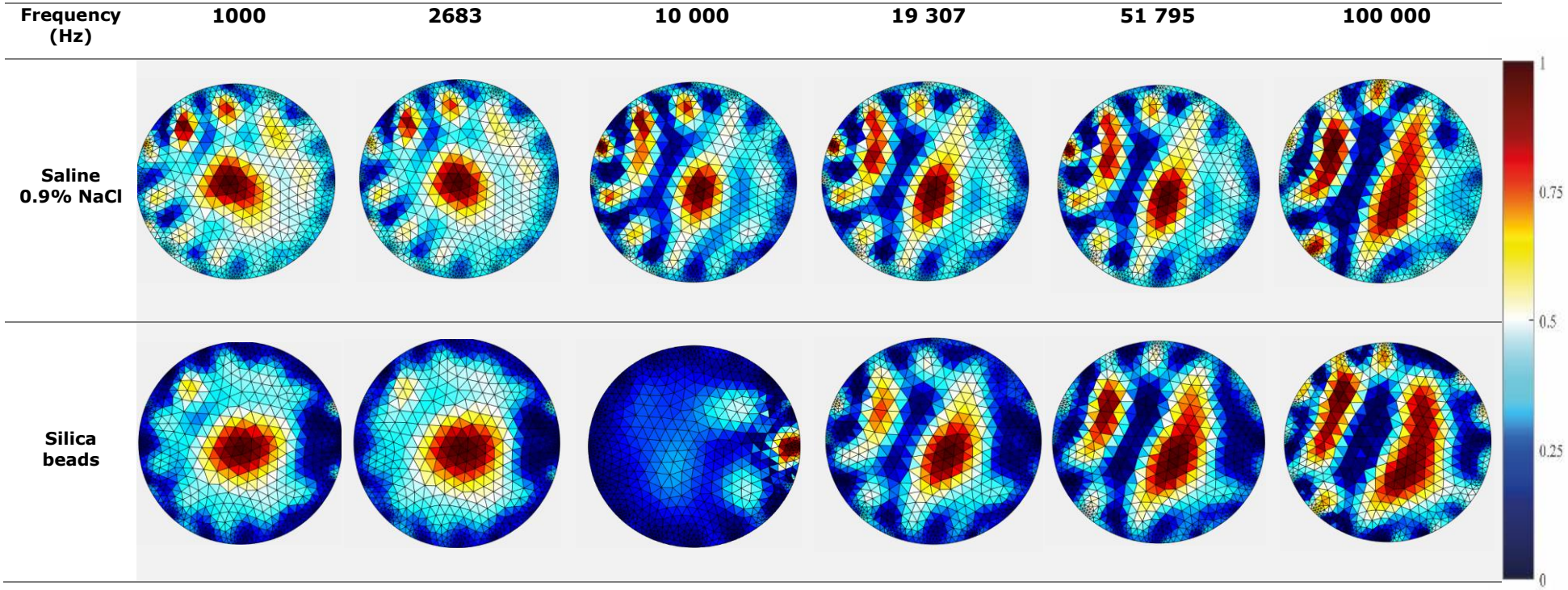

Figure 14 Shows absolute tomography images of the Silica beads and Saline solution (0.9 % NaCl). *The images are normalized between 0-1, which means red is more conductive and blue is less conductive.*

In order to test the resolution of the reconstructed images, Si-beads were tested with a 2 mm diameter chamber sensor. The average size of Si-beads is approximately 200 µm and were imaged within a 2 mm diameter EIT sensor. So, the ratio is 1:10. Assuming linear scaling, it is anticipated that dots in the reconstructed EIT image referred to the beads. Optical images and EIT images were compared. Beside of that, particle analyses of the images were performed using software program ImageJ®. In **Figure 16**, the optical image and the reconstructed EIT image of Si-beads are shown. The Si-beads are clearly seen as dots in the optical image. Furthermore, after postprocessing this image in ImageJ® software, the places of the beads are recognizable. That corresponds with the differential reconstructed tomography image, where the beads are also noticeable. It was challenging to put the particles on one place into the sensor to analyse the data due to their small sizes.

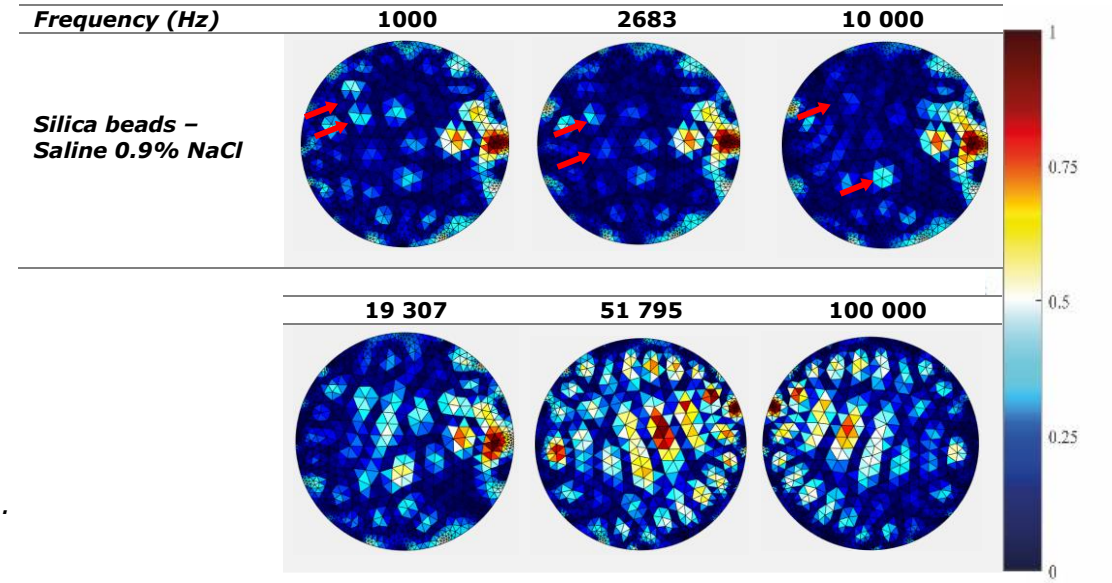

Figure 15 Differential tomography images of Si-beads. *Data of Si-beads were substracted from data of Saline Solution. Red arrows indicate the Si-beads.*

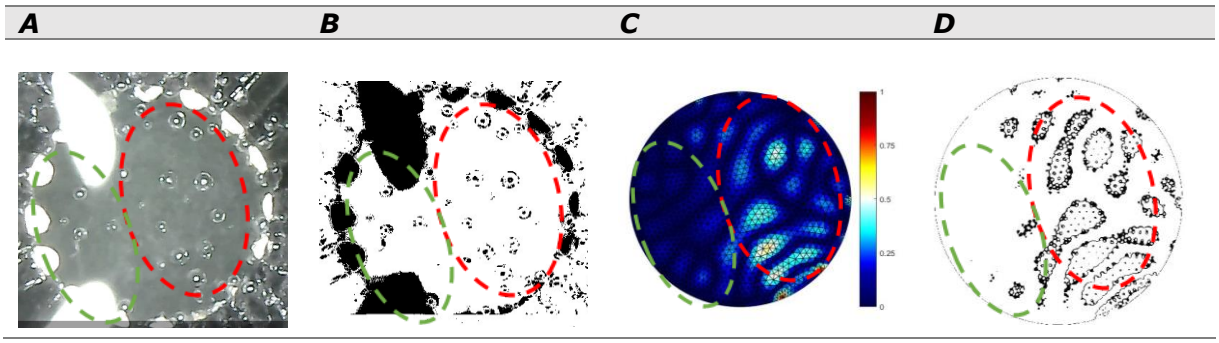

Figure 16 A 2 mm sensor with within Si-beads. The beads are more visible and distributed in the red circle than in the green circle. A*: Optical image of the sensor.* ***B****: Reconstructed image using ImageJ® software.* ***C****: Reconstructed tomography image (differential image; 1 mA @ 8kHz).* ***D****: reconstructed image using ImageJ® software of the tomography image.*

1.2 EIT of electrically conductive silicone

A conductive material has been used to test the EIT sensor. Electrically conductive silicone (NuSil R2637) was prepared according to the protocol of the company in the lab and placed on the top of the chip where 16 electrodes are located **(Figure 17)**. The material was added in both sensors with 6 mm and 2 mm in diameter, this to test how electricity will be distributed within the medium.

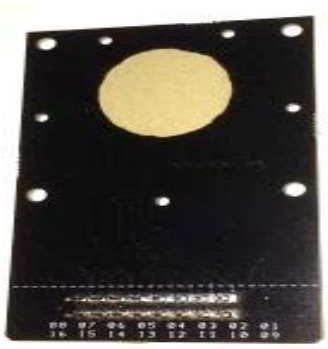

Figure 17 *a picture of EIT sensor where the electrically conductive silicone was pasted.*

This material has a resistivity of 0.01 Ωcm [27]. Due to this property, low resistivity and perfect distribution of the particles onto the sensor, the current will go through the simplest path **(Figure 18**. Note that the values of the tomography images are normalized between 0-1, this means that the red colour is more conductive. That indicates thus the current path through the electrodes, which is the simplest way to go through the sensor due to the distribution of the silicone particles. That confirms that EIT is more sensitive to conductivity changes near the electrodes than to changes far away from the electrodes.

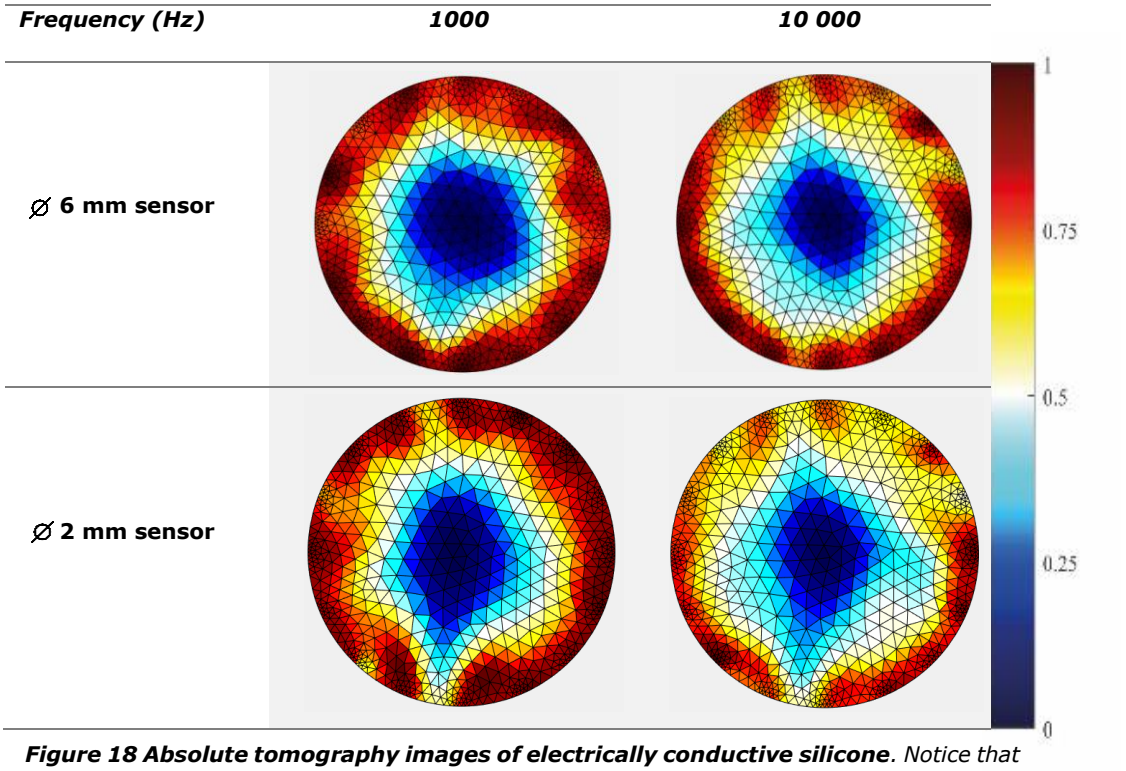

***Figure 18 Absolute tomography images of electrically conductive silicone**. Notice that the conductivity higher is along the electrodes, which indicates that the homogeneity distribution of the particles in the sensor.*

1.3 Linear measurements

In order to test whether the linear measurement method can be used with the developed setup, a simple proof-of-concept has been made. A conductive object was placed on different places onto the container. The reconstructed images show a different colour on the place where the object has been placed **(Figure 19)**. Furthermore, the Wenner method gives few data points. To solve this problem, Wenner-Schlumberger method has been used and applied where more data points can be obtained and thus the conductivity distribution can be better estimated. Unfortunately, the obtained data could not be post processed, because a suitable script was not available in MATLAB to reconstruct the image using the Wenner-Schlumberger method. Using this method, a more accurate image is expected. This method will be useful by measuring blood vessels behaviour in clinical applications.

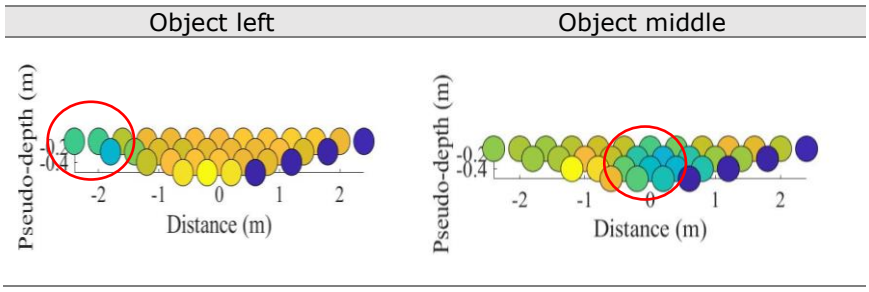

***Figure 19 The reconstructed images of the linear measurements**.Red circles show places where the objects where places.*

2 Impedance measurements and EIT of yeast cells

In order to monitor cell proliferation, *S. cerevisiae* (Dr. Oetker) was used as proof-of-concept instead of animal cells. *S. cerevisiae* is a species of yeast and is widely used in different domains, such as food industry, for baking and brewing and for making wine and spirits. Recently, it has been also used in pharmaceutical industry for scientific research. These cells are unicellular eukaryotic, single-celled micro-organisms. They belong to the taxonomy of fungus kingdom and their size can vary from 3-10 µm [10]. These yeast cells are known due to their unique properties such as high growth rate in nutrient media and does not require special labs for investigation. Therefore, they were used to monitor the cell proliferation among the electrodes of the developed EIT sensor. Different studies have shown the possibilities of monitoring the cell growth such as counting cells using a hemacytometer or by advanced electronic cell counter, but this technique does not distinguish living cells from dead cells and the results are thus more subjective [28]. When cells will be added into the EIT sensor and start to proliferate, boundary measurements will change which will lead to variation of the conductivity distribution, and these changes can be followed in function of time.

Yeast cell growth follows an obvious pattern and can be divided into four phases: the lag phase, the log phase, the stationary phase and the death phase. During the lag phase, the cells just adjust to the environment. In the log phase, the yeasts show a rapidly growth where the cells proliferate. Next, in the stationary phase, no growth occurs due to high waste concentration of complete substrate nutrients. Finally, the death phase, cells cannot survive in their environment **(*Figure 20A*)**. This pattern can be obtained when the mean values of the boundary measurement along the electrodes of the EIT sensor will be plotted in function of time.

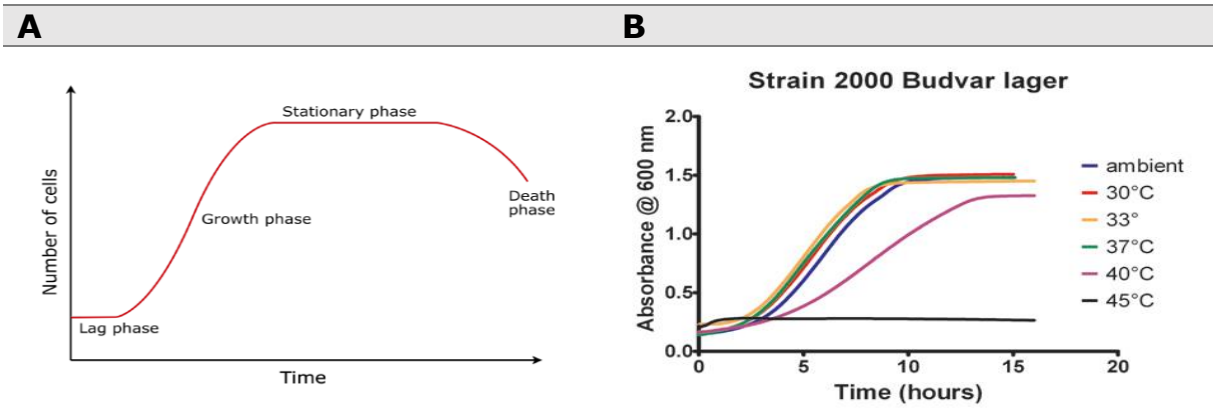

Figure 20 Properties of yeast cells. A: *Shows the four phases of yeast growth.* ***B:*** *Shows the temperature dependency of yeast proliferation* [29].

During the internship, two different culture media has been used, 10% glucose and a combination of 1% agar in 10% glucose. The yeast cells were kept in a culture oven with a temperature of 33°C. This temperature has been chosen because it shows a normal growth curve of yeast cells **(*Figure 20B*)** [29].

2.1 Monitoring the culture of yeast cells

The impedance measurements on yeast cells were performed using two devices, Agilent 4284A and MUSEIC V2.0. When the cells are added into the sensor, a known current will be injected. Afterwards, the potential boundary values along the electrodes will be measured. The obtained data are loaded in EIDORS library to reconstruct tomography images. Before the solver can calculate the corresponding images of the measured boundary potential values, an accurate model of the physical setup is needed. One drawback when Agilent device is used is that it takes approximately 14 minutes for a full set of data at one frequency compared to MuseicV2.0 which needs only 56 seconds for one set of data. This will lead for missing some cell behaviour by measuring the cell proliferation in function of time. Therefore, another impedance analyser, which measures the boundary voltages at a higher sampling rate, will be used. Furthermore, a finite element method (FEM) is used to solve the model. It represents a well filled with culture medium with cells on it **(Figure 21A)**. However, this 3D model is not used to solve the inverse problem, another simplified alternative model is taken **(Figure 21B)**. The medium is assumed to be constant in the z direction, this is the height of the culture chamber. When these variabilities are eliminated, a new 2D image is reconstructed. Note that the domain of the model is discretised into small elements (e.g. tetrahedral elements), where the measured boundary potential values can be fitted. The electrodes are represented as dots along the circular model. It is thus important to know the position and the dimension of the electrodes in detail to avoid noise in the reconstruction images as referred in literature, it should not give a problem in our case [30].

When the conductivity matrix is based on only one data set of the boundary measurement, the minimalistic changes of impedance during the process during cell growth cannot be detected, which make this problem one of the difficulties when using the principle of EIT on cellular growth. This can be solved by taking differential measurement and feed this data into the EIT algorithm. One data set will be used as reference, in this case data of the culture medium and other data sets when the yeast cells are growing. By subtracting these two data sets, only the behaviour of the yeast cells can be studied and monitored. However, glucose can evaporate because a small volume of yeast growth medium is used. This can be prevented by using a constant flow of the medium into the flow cell. Nevertheless, the yeast cells can be flushed away after flushing the medium into the sensor. Therefore, further validation is needed by using a microscope during the flushing to check whether the cells are still in the sensor. On the other hand, agar will be performed as culture medium. This medium will not degrade over time which will be benefit for the measurement and external influences will be excluded.

The One Step Gauss Newton solver was selected as the preferred inversion method in the script for the reconstruction of the images. Laplace prior was chosen as filter. The hyperparameter is a regularization factor in the reconstruction algorithm and is kept constant in each iteration to compare the same images. This parameter has a significant impact on the reconstructed images. Although different methods exist to address this problem, this parameter is manually chosen for each image in this thesis [31]. The hyperparameter was not calculated using the method due to the intensive mathematical calculation that the algorithm has to do. By approximation of this hyperparameter, images will be reconstructed and analysed faster in MATLAB.

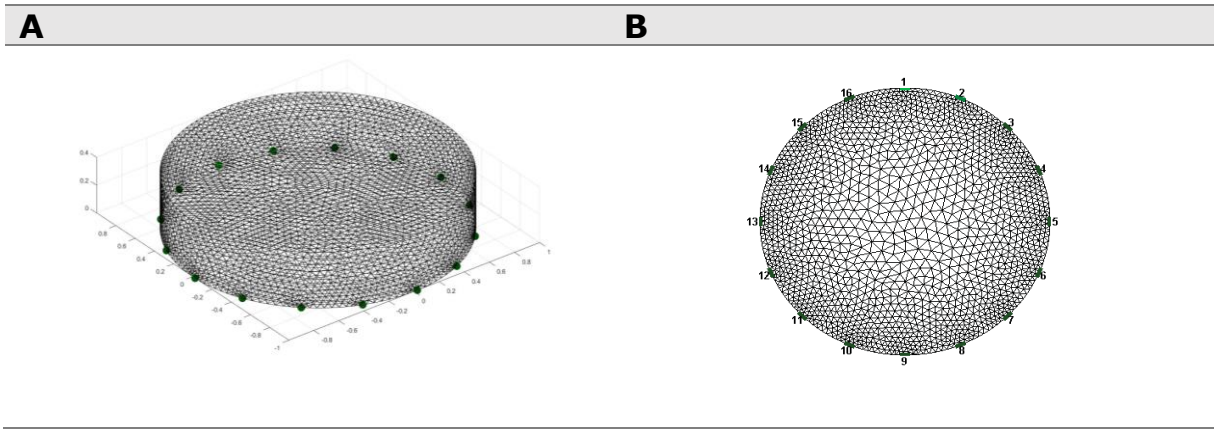

***Figure 21 Model where the data will be fitted**. A: 3D FEM. B: 2D FEM. (FEM: Finite element model).*

2.2 Impedance measurements of yeast cells

In order to establish whether yeast cells are detectable with the developed sensor and to see whether they are more or less conductive than the used culture medium, the impedance of pure culture medium (10% glucose) and a combination of both were measured using the EIT sensor with a 6 mm diameter. A two-electrode configuration has been used to measure the impedance. In this case, the two farthest electrode, E1 and E9 has been chosen. A current of 10 mA has been applied through the sensor. The impedance spectra (magnitude and phase) were measured between 1 kHz and 100 kHz.

A clear difference between the two samples in the impedance values is detected **(Figure 22)**. The culture medium with yeast cells shows a lower magnitude, which indicated that yeast cells are more conductive than 10% glucose as found in previous study [17]. That is important to know in the next sections, when the tomography images of yeast will be analysed. Moreover, it explains that EIT imaging technique is able to follow the yeast cells into the culture medium.

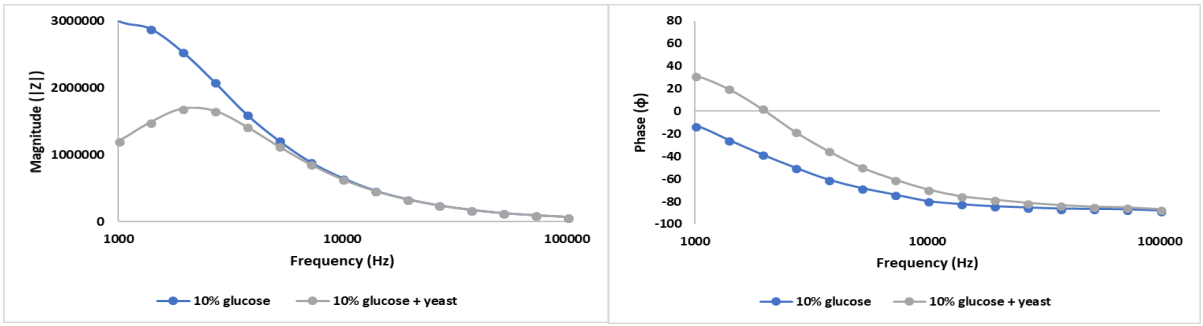

Figure 22 Both the magnitude and phase are shown for culture medium and a mixture of culture.

2.3 Detection of yeast grains with EIT sensor

Different amount of yeast grains is added in function of time to see whether there is a difference in the mean values of the boundary measurements. A culture medium consists out of 1% agar in 10% glucose was prepared and a volume of (+/- 100 µL) was added to the culture chamber of the sensor. The measurements were performed after 2 hours from the moment of preparing agar. This is

important because when the agar begin to solidify, the magnitude will increase and afterwards it remains constant **(Figure 23)**. Therefore, it is important to do the measurement after this phase of solidification.

Both setups, Agilent and MuseicV2.0, were connected with a 6 mm diameter sensor. Hereby, respectively, 8 electrodes and 16 electrodes were used. The experiment was performed as follow: first 10 minutes, only measurement of agar was performed. Next, one grain of yeast was added to the sensor and have been measured for 10 minutes. Further, 3 grains were measured with the sensor. And at last, the sensor measures the 10 added grains. Note that the mean value of the magnitude increases **(Figure 24)**, after adding grains on the top of the sensor. Since the EIT sensor is miniaturized, yeast grains will be used because they are considered as a more conductive object in comparison to the culture medium.

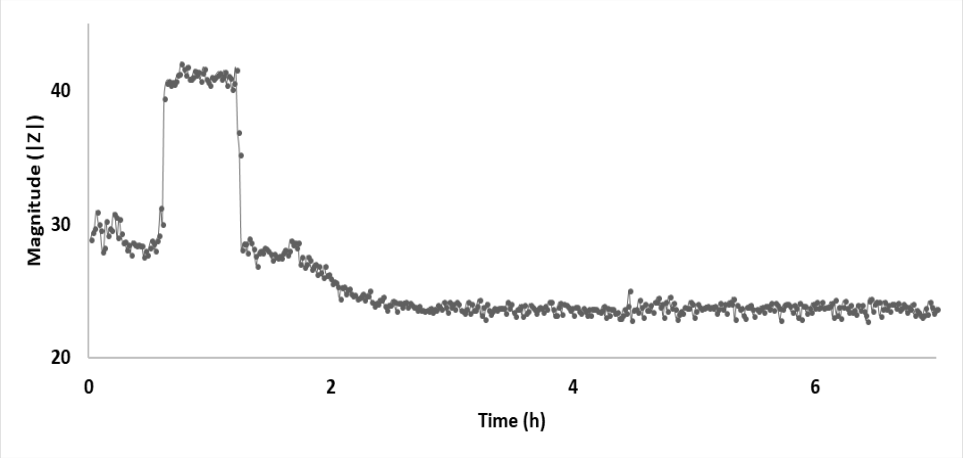

***Figure 23 Mean value of impedance measurements over time**. The used culture medium was 1 % agar in 10 % glucose. (Museic V2.0; Adjacent method)*

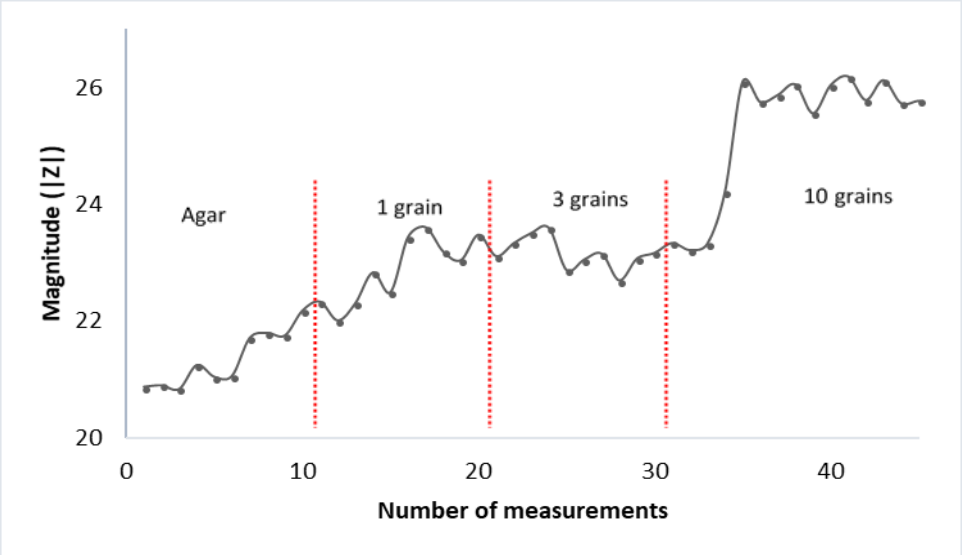

***Figure 24 Mean value of impedance measurements over time.** The increases show that the conductivity changes at the surface.*

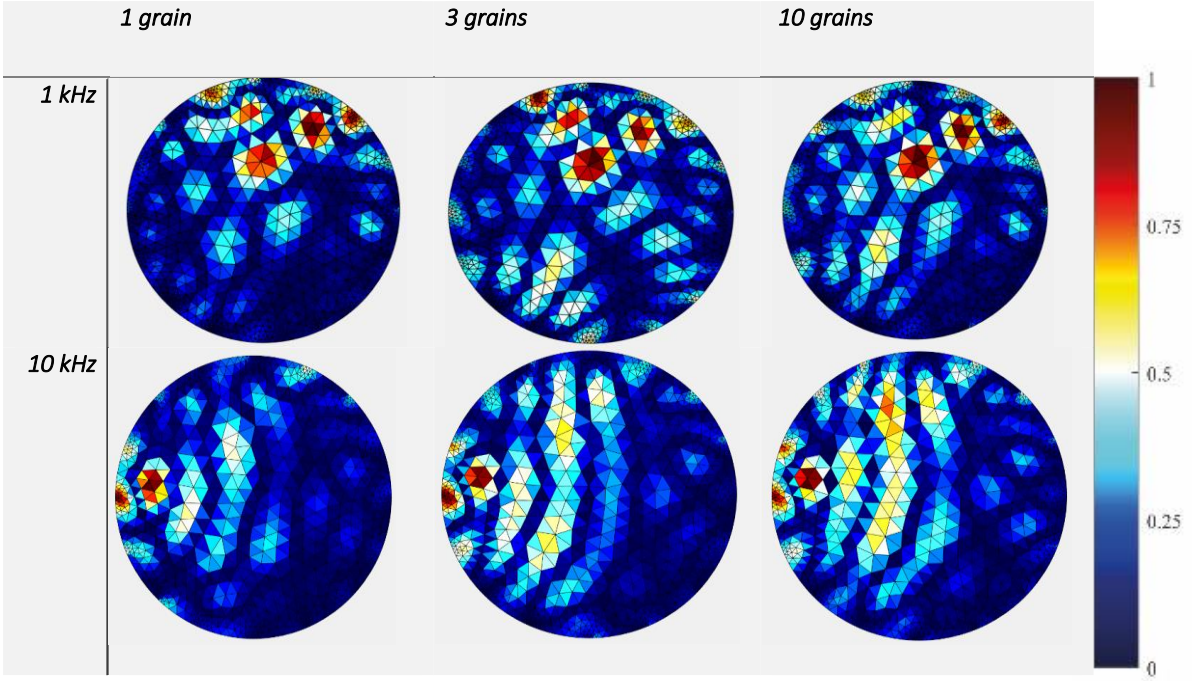

***Figure 25 Tomography images of yeast grains in the EIT sensor**. The more yeast are added, the more red the tomography image.*

The same experiment was performed by Agilent and for this differential tomography images were reconstructed of the different amount of yeast cells. Note that the more yeasts grains covered the sensor, the redder the image, the more conductive. The images were performed at two different frequencies **(figure 25)**.

2.3 EIT of yeast colonies

For this section, a yeast grain was placed on the top of the sensor. The sensor was filled with a 1% agar medium. Two data sets were obtained, the first data was at the moment of placing the yeast and the other data set was after 16 hours. The behaviour of yeast cells was studied.

For the reconstruction algorithm, Gauss Newton solver has been used with the combination of priors and method to calculate the hyperparameter to look which combination gives the best conductivity image. Therefore, the algorithm scheme **(figure 7)** has been used. In this script every possible combination for hyperparameter calculation and the prior selection is possible. With this, 16 images where obtained. The optical image of the sensor shows that colonies are formed. The images generated from the inversion process appear to include centrally located decreases in conductivity, which is indicative for colony. After 16 hours, the yeast grain began to form colonies in the sensor. These colonies, represented as red regions, are detectable in the tomography images **(figure 26B)**. The images demonstrate that EIT technique is a promising tool to detect changes on the surface of the sensor. An optical image of the sensor was taken and illustrates the place of the grain yeast **(Figure 26A)**.

These results were comparable with *T. Sun et al*. whereby they *Physarum Polycephalum* as cellular organism to test their EIT sensor [6]. They have also used a circular 16 electrode culture chamber. However, the hyperparameter in this section was calculated using the different methods together with different prior solver. While in their case, this value was manually chosen.

A **B**

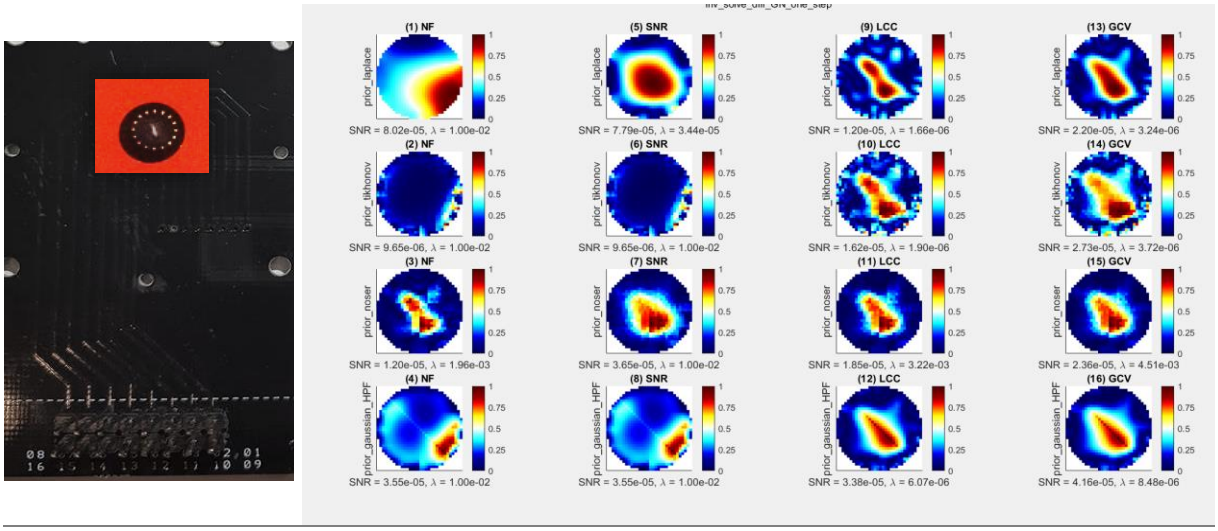

Figure 26 Yeast grain followed using EIT sensor. A: *Optical picture of the sensor.* ***B:*** *Resulting images when placing a yeast grain in the middle of the sensor. The red area in the middle indicated the proliferation of yeast and forming of the colonies. The conductivity values are normalized between 0-1.*

A **B**

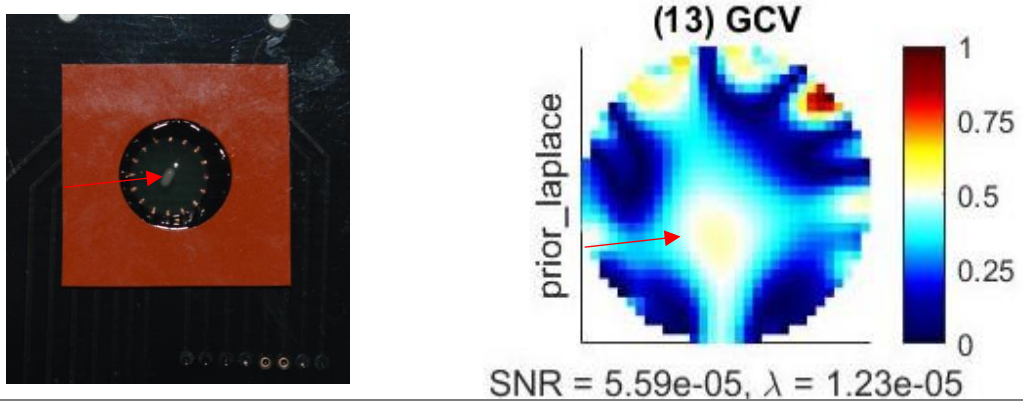

Figure 27 Yeast grain on the sensor. A: *Optical picture of the EIT sensor with a grain in the middle of it (red arrow).* ***B:*** *Reconstructed image using the combination algorithm of calculating the hyperparameter. The yellow colour indicated the place where the grain is (red arrow).*

2.4 Detection of different yeast concentration with EIT

The next investigation is to image dissolved yeast cells in culture medium via developed EIT sensor. A series of different concentrations of yeast in a 10% glucose culture medium have been prepared to investigate at which concentration that the EIT sensor is sensitive enough. A high concentration ensures that the cellular growth will be detected difficulty because the sensor surface will be covered in this way. A current was injected into the sensor and potential measurements with Agilent were

taken to make tomography images. Firstly, the raw data of the culture medium and a concentration of 8 grains/ml yeast cells were plotted to see whether any difference in the measured magnitude. As seen in **figure 27**, a clear difference in magnitude is observed. The culture medium measurements demonstrate a higher impedance than medium with yeast cells. This indicates that the yeast cells have a higher conductivity value than the culture medium, and it promises also that tomography images can be perceived. Beside of that, light microscopy images were taken to compare it with the obtained reconstructed images. Hereby, a low concentration of 2 grains/ml yeast cells is enough to study the cells.

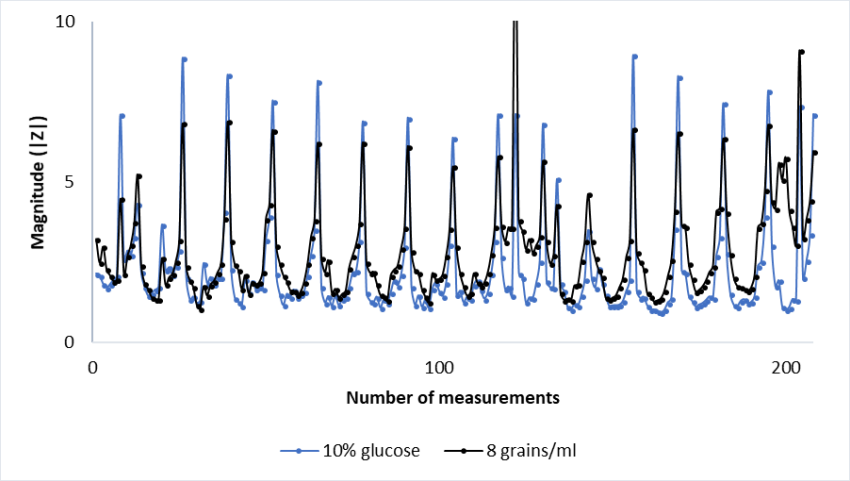

***Figure 27 Raw data of culture medium (10% glucose) vs 8 grains/ml of yeast cells**.. Note that the magnitude of glucose is higher compared to the yeast, which indicates that yeast more conductive is that glucose. (10 mA @ 10 kHz)*

As expected, the lower the concentration of yeast cells, the lower the conductivity value **(Figure 28)**. The values of the colour bar are normalized between 0-1, which means that the red region is more conductive, and the blue is more resistive. Next, the higher the concentration, the redder colour in the images, which indicates more cells. Note also that measurements performed in both sensors, with two different diameters, gave similar results. Unfortunately, single cells of yeast are very difficult to observe with this EIT sensor, because the ratio between the diameter of the sensor and the yeast cell is around 1:200. It is possible to detect them when the EIT sensor is further miniaturized. In this way, the ratio of the single cell and the diameter of the sensor will be increased.

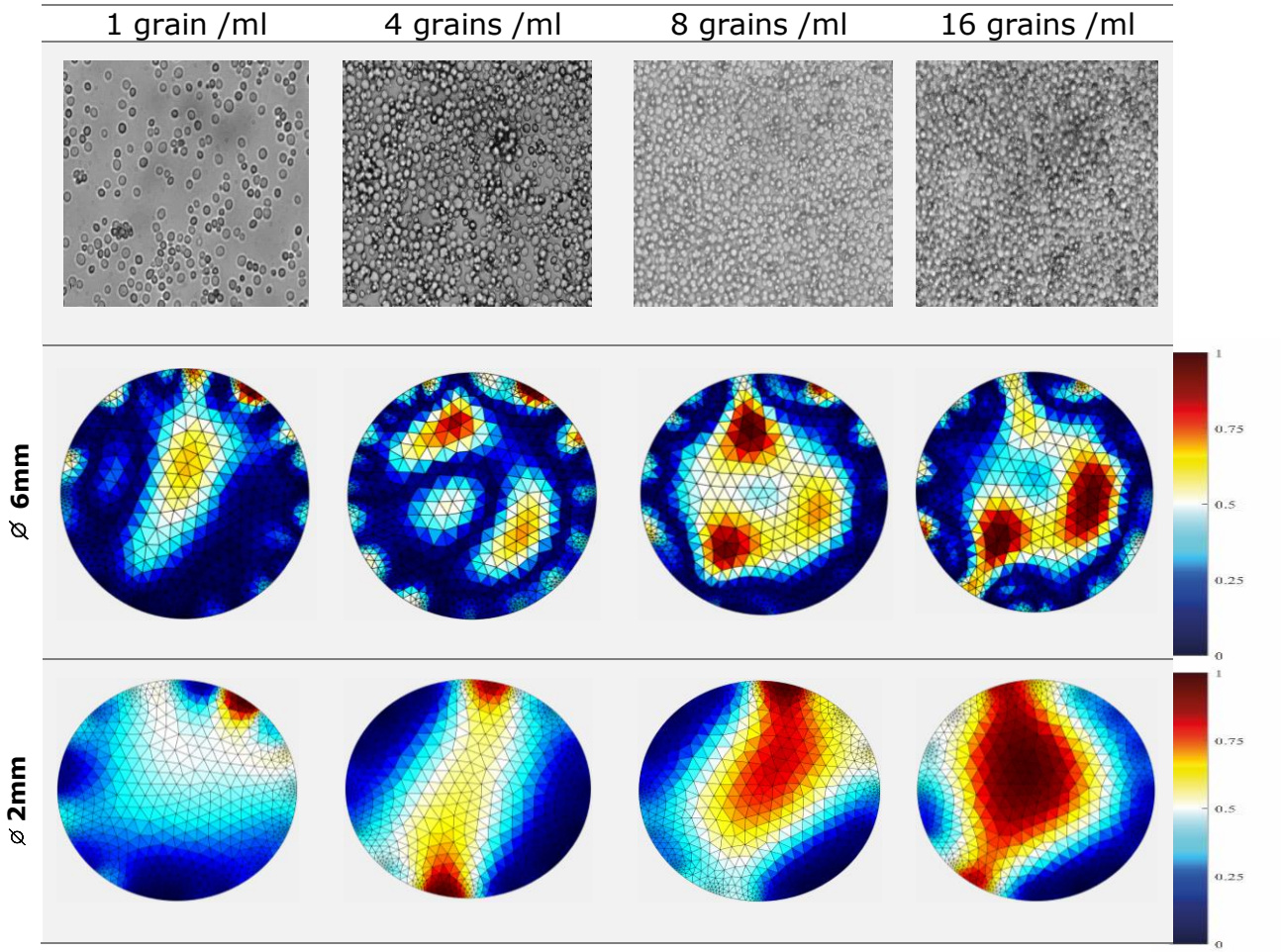

Figure 28 Tomography images of different concentration of yeast cells dissolved in 10% glucose *(**First row**) Microscopy images of yeast cells. **(Second row)** Reconstructed EIT images of two different sensors (6 mm). Differential images, the higher the yeast concentration, the higher the conductivity distribution. **(Third row)** sensor with (2 mm) gives clear expected results.*

2.5 Yeast cells monitoring in function of time

Variation in yeast concentration in a very low concentration lead to changes in values of the conductivity of the reconstructed images as illustrated in previous section. These findings indicate that the higher the concentration of yeast, the higher the conductive distribution of the image. Furthermore, the yeast cells show a lower magnitude in impedance compared the cell culture medium **(figure 27)**. Hence, this indicates that when the yeast cells will proliferate, the number of cells will increase and thus automatically, the conductivity will increase. These changes can be followed using an EIT sensor. From this hypothesis, the following experiment is performed. Yeast suspension of a concentration of 2 grains/ml were dissolved in 10% glucose in an Eppendorf tube. The cell growth was followed in this tube by adding an amount of 100 µL of the solution to the EIT sensor at different times in the culture chamber of the sensor. Before the solution was taken, the tube should be stirred to get a homogeneous distribution of the yeast cells in the solution. The Eppendorf tube was placed in the culture oven on a temperature of 30°C to keep yeast in normal environment of growing.

The results show that the conductivity increases in function of time, which indicated the cell proliferation and the cell division **(figure 29)**. After 1 hour, a red region is remarkable, indicates the cell division of yeast cells. Note that the cells are death after 24 hours, which is obviously remarkable with the blue colour, which means a decrease in conductivity and induction of cell death.

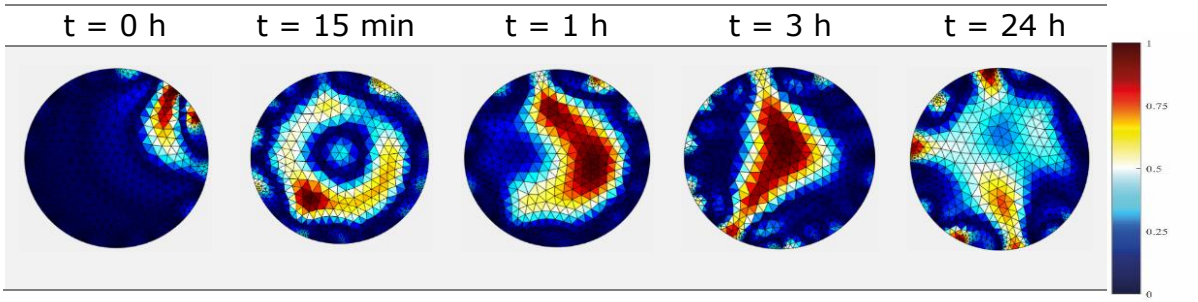

Figure 29 Reconstructed tomograpy images of yeast cells in function of time*. The yeast cell proliferation induce a higher conductivity, thus there is more red region obtained in the reconstructed images. Note that after 24 h the cells are death, and the image is more bluer. Data were taken at 1 kHz (sensor 6 mm).*

2.6 Yeast cell growth measurements in real-time

The proliferation of the yeast cells will be followed in real-time after adding these cells in the sensor which was integrated in the flow cell. However, the hardware device gave errors during the measurement. Because the measurement could not measure the boundary measurements and block midway due to an unknown reason. This lead for missing some data. After several attempts, this experiment is successfully completed and gave the expected results where the four phases of yeast cell can be recognised **(Figure 20A)**. A culture medium of 1% agar and 10% glucose was prepared and was added to the sensor. After two hours, yeast cell suspension of a concentration of 5 mg/ml was added to the EIT sensor. The measurements were conducted overnight in an incubator with a temperature of approximately 30°C. The sensor was connected to the Agilent that measures the boundary measurement by using both the adjacent method. By the adjacent method the driving electrodes were excluded during the measurement. The average value of each frame and plots of these values for the total time span, results into the following curve progress **(figure 30C)**. A clear trend is shown during the proliferation phase followed by the phase of cell death; this curve is comparable with the growth curve **(Figure 20A)**.

The cell proliferation will generate a change in the conductivity matrix which are detectable in the images. However, the drawback of the EIT technique is that small changes in the measured voltages due to the sensitivity to environmental noise. Whereas it is very difficult to find the optimal solution for this. As aforementioned, that can be solved by taking difference between the two data set and feed this data into the EIT algorithm. The high transport capacity of proteins through the protein pumps in the cell barrier leads to changes in the homeostasis of the yeast cells [10].

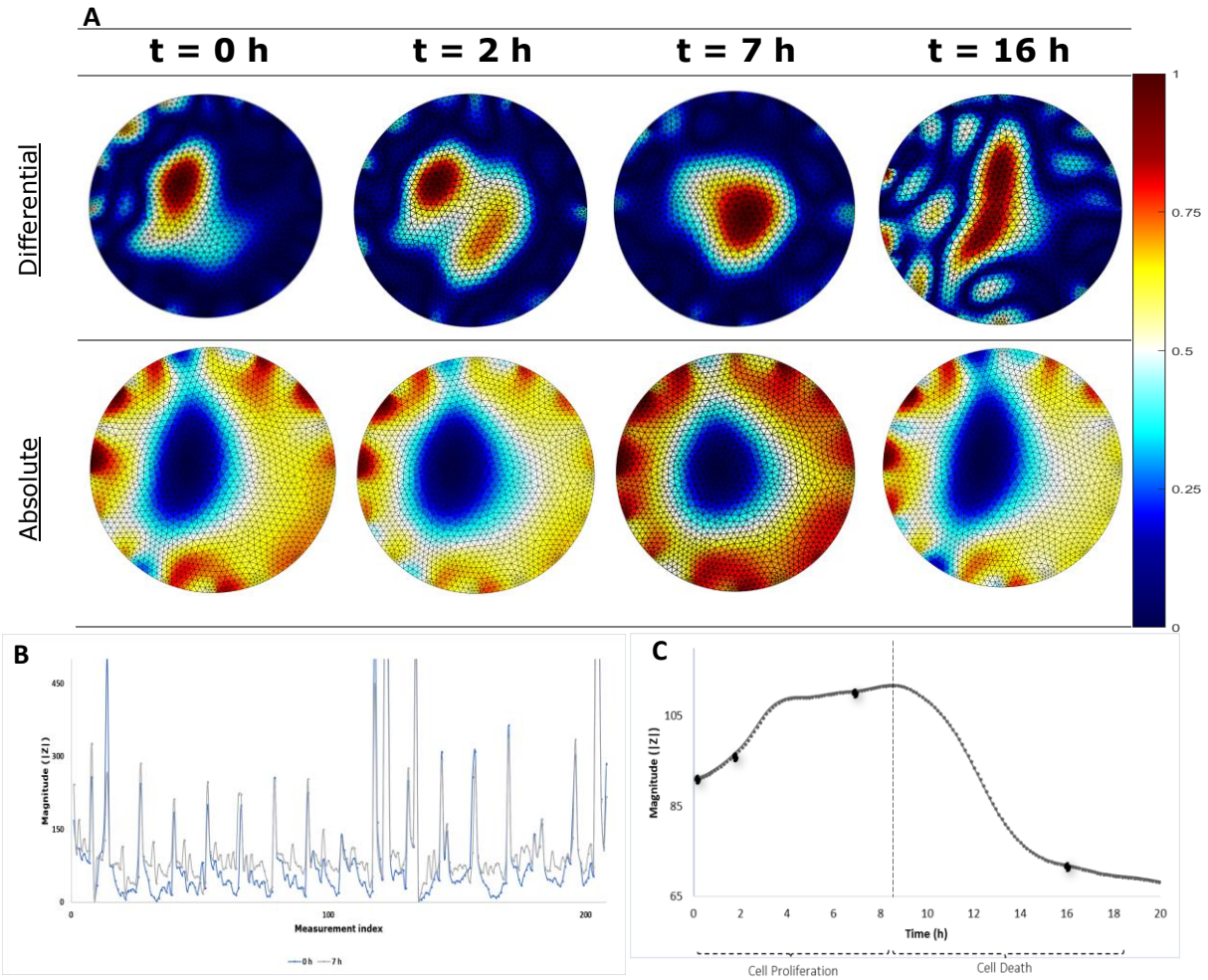

Figure 30 An overview of monitoring yeast cells in real-time A: *The EIT image at t = 0 h shows the starting point of the growing curve in function of time. The progression of the growth curve is shown at several intervals: 0 h, 2 h, 7 h and 16 h.* ***B:*** *an overview of the measured magnitude is shown for each frame.* ***C:*** *Taking the mean value of each frame and plotting these values for the total time. A clear trend is shown during the proliferation phase followed by the phase of cell death. The dots in the graph corresponds the reconstructed images in A.*

The 2D-Laplace algorithms in EIDORS library were used for image reconstruction and the used parameters **(table S1)**. The conductivity changes of yeast cells in 2D can be estimated by using this algorithm with the developed miniaturized EIT sensor **(Figure 29 and 30A)**. Based on initial experiments results, the intensity changes are dependent on the conductivity of the yeast cells. 2D EIT images are reconstructed by obtained colour difference between non-conductive and conductive yeast cells. Further, the Laplace prior demonstrated a superior image quality, a noise reduction performance and a location estimation compared to other priors **(Figure 26B).** The results were comparable with other studies where better results were obtained by using Laplace in stead of the Tikhonov prior [20].

During this study 2D image reconstructions of cells by the EIT system was characterized. Although, further investigation on 3D image reconstructions should be performed to obtain a better view on cell behaviour resulting in a better interpretation of cell-drug respones.

Recent studies of cell-drug responses by using EIT have proved that a suitable EIT algorithm system produces stable and high-quality images of 3D cellular substances. However, another study has proved that EIT can be used to detect cancer cells in an early stage. Nowadays, the drug discovery is complicated and time-consuming. Therefore, it is a challenge to develop robust, fast, cost-efficient methods to profile potential drugs. Preliminary results have demonstrated that a rapid cell-drug response image is feasible by using EIT [33]. They have studied and investigated the interaction between MCF-7 human breast cancer cell spheroid and diluted Triton X-100 solution. This is a common drug that kill cancer cells by lysing and permeabilizing the membranes of living cells [34].

IV Conclusion

The aim of the current research is to execute a feasibility study on how EIT imaging can help in the analysis of the cell-drug/biomaterial interaction. This is accomplished by creating a new platform that was able to image cells in culture by making use of impedance measurements. Regarding to this, a new miniaturized EIT sensor consisting out 16 electrodes with custom hardware was developed. Two different sensors with two different diameters have been designed. These sensors were integrated in a flow cell to create a culture chamber where the cells can growth. Furthermore, custom hardware, the Agilent 4824A has been programmed to be able to switch between the 16 electrodes. The increased number of electrodes, compare to previous study [17] will provide an improvement in the positional accuracy to reconstruct an image [31].

Several studies have investigated the EIT on cellular imaging [29,35]. The big difference with our study is the use of a miniaturized sensor which contains 16 electrodes and the use of optimized script for the image reconstruction.

On the one hand, this study was focused on the development of the setup. Hereby, the characterization of the setup, based on different experiments, was accomplished. Next, tomography images of the thorax and the bladder has been taken using the system. The results have confirmed that the system is capable for operation. On the other hand, the EIT sensor has been tested using different materials with different conductivity values. For this experiment, Si-beads and electrically conductive silicone have been used.

During all the measurement, the EIDORS library was used to reconstruct the images. One solver and one prior has been chosen for the most images. Furthermore, the hyperparameter during the image reconstruction has been empirically chosen. Beside of that, an algorithm was programmed by combining different models and cross-analysing variables to achieve the best spatial conductivity image. This algorithm requires an intensive calculation. The last aims of this internship were focused on yeast measurement. Yeast growth was monitored using the new system. The results have shown that yeast cells can be monitored in a very low concentration range. Furthermore, the cell colonies in function of time was visible in the tomography image. Based on these results, the applicability of EIT as an alternative way for analysing the cell behaviour is proven. By obtaining a working setup for tomography, based on a non-invasive, contact less way. Another advantage of EIT technique will be further focused in the reconstruction of a 3D images.

The findings of this study have a number of important implications for future practice. Therefore, the EIT sensor can even be miniaturized further, by making the electrodes in a very small sizes using the lithography technique. In this way, a very small culture chamber will be created which even can study single cells in microscopic scale. This will make a bridge to a new, handy, cheap setup in the research field and will accelerate the development of new drugs, by studying cell-drug interaction whether the drug induce a conductivity change on cells. These findings provide more insights for future research on cellular behaviour. This system provides a non-invasive lab-on-chip technology for spatial mapping of the electrical properties of single cells, which will be significant and useful for diagnostic and clinical applications.

References

[1] A. Adler and W. R. B. Lionheart, "Uses and abuses of EIDORS: An extensible software base for EIT," *Physiol. Meas.*, vol. 27, no. 5, 2006.

[2] A. V. Naumova, M. Modo, A. Moore, C. E. Murry, and J. A. Frank, "Clinical imaging in regenerative medicine," *Nat. Biotechnol.*, vol. 32, no. 8, pp. 804–818, 2014.

[3] J. D. Bryers, C. M. Giachelli, and B. D. Ratner, "Engineering biomaterials to integrate and heal: The biocompatibility paradigm shifts," *Biotechnol. Bioeng.*, vol. 109, no. 8, pp. 1898–1911, 2012.

[4] L. D. L. L. De Matos *et al.*, "Biomarker Insights Immunohistochemistry as an Important Tool in Biomarkers Detection and Clinical Practice," *Biomark. Insights*, vol. 5, pp. 9–20, 2010.

[5] T. K. Bera, "Applications of Electrical Impedance Tomography (EIT): A Short Review," *IOP Conf. Ser. Mater. Sci. Eng.*, vol. 331, no. April, p. 012004, 2018.

[6] T. Sun, S. Tsuda, K. P. Zauner, and H. Morgan, "On-chip electrical impedance tomography for imaging biological cells," *Biosens. Bioelectron.*, vol. 25, no. 5, pp. 1109–1115, 2010.

[7] E. Kyriacou, S. Christofides, and C. S. Pattichis, "XIV mediterranean conference on medical and biological engineering and computing 2016: MEDICON 2016, March 31st–April 2nd 2016, Paphos, Cyprus," *IFMBE Proc.*, vol. 57, pp. 1259–1260, 2016.

[8] Y. Mermoud, M. Felder, J. D. Stucki, A. O. Stucki, and O. T. Guenat, "Microimpedance tomography system to monitor cell activity and membrane movements in a breathing lung-on-chip," *Sensors Actuators, B Chem.*, vol. 255, pp. 3647–3653, 2018.

[9] J. P. Wikswo *et al.*, "Engineering challenges for instrumenting and controlling integrated organ-on-chip systems," *IEEE Trans. Biomed. Eng.*, vol. 60, no. 3, pp. 682–690, 2013.

[10] V. Volkov, "Quantitative description of ion transport via plasma membrane of yeast and small cells," *Front. Plant Sci.*, vol. 6, no. June, pp. 1–22, 2015.

[11] S. Haltiwanger, "The electrical properties of cancer cells," *Wind Power, 17.06*, 2010.

[12] T. Faes, H. Van der Meij, J. de Munck, and R. Heethaar, "The electric resistivity of human tissues (100 Hz-10 MHz): a meta-analysis of review studies The electric resistivity of human tissues (100 Hz – 10 MHz): a meta-analysis of review studies," *Physiol. Meas*, vol. 1, no. 20, pp. R1–R10, 1999.

[13] J. Hinz, "Electrical Impedance Tomography," *Curr. Respir. Med. Rev.*, vol. 5, no. 2, pp. 105–109, 2009.

[14] B. H. B. and I. l. F. D.C. Barber, "IMAGING SPATIAl DISTRIBUTIONS OF RESISTIVITY USING APPLIED POTE~TIAl TO~10GRAPHY - APT," no. 12, pp. 446–447, 1984.

[15] Y. Zhang, R. Xiao, and C. Harrison, "Advancing Hand Gesture Recognition with High Resolution Electrical Impedance Tomography," *Proc. 29th Annu. Symp. User Interface Softw. Technol. - UIST '16*, pp. 843–850, 2016.

[16] T. K. Bera and J. Nagaraju, "A MATLAB-Based Boundary Data Simulator for Studying the Resistivity Reconstruction Using Neighbouring Current Pattern," *J. Med. Eng.*, vol. 2013, pp. 1–15, 2013.

[17] M. Lemmens, W. De Raedt, L. Grieten, and R. Thoelen, "Electrical impedance tomography with a lab-on-chip for imaging cells in culture," vol. 50, no. 1, p. 3590, 2015.

[18] S. L. Swisher *et al.*, "Impedance sensing device enables early detection of pressure ulcers in vivo," *Nat. Commun.*, vol. 6, pp. 1–10, 2015.

[19] R. Avill *et al.*, "Applied Potential Tomography: A New Noninvasive Technique for Measuring Gastric Emptying," *Gastroenterology*, vol. 92, no. 4, pp. 1019–1026, 1987.

[20] Y. Yang, J. Jia, S. Smith, N. Jamil, W. Gamal, and P. O. Bagnaninchi, "A miniature electrical impedance tomography sensor and 3-D Image Reconstruction for Cell Imaging," *IEEE Sens. J.*, vol. 17, no. 2, pp. 514–523, 2017.

[21] P. Sentenac, G. Jones, M. Zielinski, and A. Tarantino, "An approach for the geophysical assessment of fissuring of estuary and river flood embankments: Validation against two case studies in England and Scotland," *Environ. Earth Sci.*, vol. 69, no. 6, pp. 1939–1949, 2013.

[22] J. Punter-Villagrasa, J. Cid, J. Colomer-Farrarons, I. Rodríguez-Villarreal, and P. L. Miribel-Catala, "Bioimpedance Technique for Point-of-Care Devices Relying on Disposable Label-Free Sensors – An Anemia Detection Case," *Biosens. - Micro Nanoscale Appl.*, p. 32, 2015.

[23] L. G. and C. Wilms, "Understanding the cell as an electtrical circuit," *Sci. Ltd*.

[24] H. Ha *et al.*, "A bio-impedance readout IC with frequency sweeping from 1k-to-1MHz for electrical impedance tomography," *IEEE Symp. VLSI Circuits, Dig. Tech. Pap.*, pp. C174–C175, 2017.

[25] T. K. Bera and J. Nagaraju, "Studying the resistivity imaging of chicken tissue phantoms with different current patterns in Electrical Impedance Tomography (EIT)," *Meas. J. Int. Meas. Confed.*, vol. 45, no. 4, pp. 663–682, 2012.

[26] E. Geophysics, I. I. Spring, and I. Electrical, "Introduction to Reisitivity," *Explor. Geophys.*,

pp. 2–5, 2003.
[27] A. Engineering, "R-2637 ELECTRICALLY CONDUCTIVE RTV SILICONE," no. December, 2006.
[28] W. Strober, "Monitoring cell growth.," *Curr. Protoc. Immunol.*, vol. Appendix 3, p. Appendix 3A, 2001.
[29] P. Held, "Monitoring Growth of Beer Brewing Strains of Saccharomyces Cerevisiae," *BioTek Instruments*, no. 18, pp. 1–6, 2010.
[30] A. R. A. Rahman, "Effect of electrode geometry on the impedance evaluation of tissue and cell culture." sensors actuators,B Chem, 2007.
[31] D. Liu, A. K. Khambampati, and J. Du, "A Parametric Level Set Method for Electrical Impedance Tomography," *IEEE Trans. Med. Imaging*, vol. 37, no. 2, pp. 1–1, 2017.
[32] R. H. Bayford, "(12) United States Patent," *U.S. Pat.*, vol. 1, no. 12, 2002.
[33] D. Koley and A. J. Bard, "Triton X-100 concentration effects on membrane permeability of a single HeLa cell by scanning electrochemical microscopy (SECM)," *Proc. Natl. Acad. Sci.*, vol. 107, no. 39, pp. 16783–16787, 2010.
[34] P. Linderholm, L. Marescot, M. H. Loke, and P. Renaud, "Cell culture imaging using microimpedance tomography," *IEEE Trans. Biomed. Eng.*, vol. 55, no. 1, pp. 138–146, 2008.
[35] B. K. Walsh and C. D. Smallwood, "Electrical Impedance Tomography During Mechanical Ventilation," *Respir. Care*, vol. 61, no. 10, pp. 1417–1424, 2016.
[36] M. Graf and T. Riedel, "Electrical impedance tomography: Amplitudes of cardiac related impedance changes in the lung are highly position dependent," *PLoS One*, vol. 12, no. 11, pp. 1–14, 2017.
[37] S. Białka, M. Copik, K. Rybczyk, and H. Misiołek, "Electrical impedance tomography for diagnosis and monitoring of pulmonary function disorders in the intensive care unit - Case report and review of literature," *Anaesthesiol. Intensive Ther.*, vol. 49, no. 3, pp. 222–226, 2017.
[38] E. L. V. Costa *et al.*, "Real-time detection of pneumothorax using electrical impedance tomography," *Crit. Care Med.*, vol. 36, no. 4, pp. 1230–1238, 2008.
[39] T. Schlebusch, S. Nienke, S. Leonhardt, and M. Walter, "Bladder volume estimation from electrical impedance tomography," *Physiol. Meas.*, vol. 35, no. 9, pp. 1813–1823, 2014.

Appendix

In this supporting information, different experiments performed on the thorax and the bladder will be discussed. Tomography images of these tissues were reconstructed using the developed setup. Furthermore, some extra information about reconstructed images in this thesis are also added.

S1 EIT of the human tissues

S1.1 EIT of the thorax

The purpose of this chapter is to introduce an overview how EIT can be used as a clinical imaging technique for human tissues. This section looks at several relevant studies which deal with the use of EIT as an imaging modality that may be useful for the quantification of lung disorders.

Biological tissues conduct electricity due to the presence of ions which acts as charge carriers. Some tissues conduct electricity better than others. For example, bone is a poor conductor while the muscle is a relatively good conductor as aforementioned in **table 1** (see introduction). Moreover, lung tissue contains air and has a resistivity which is about five times greater than other tissues in the thorax. Due to these properties, EIT is a technique that can produce images showing the distribution of the tissue conductivity and offers thus important benefits over standard imaging modalities. Also, the electrical conductivity changes as a function of changes in the lung volume during ventilation. Different studies have proved and described the applications of thoracic EIT. For examples, in the monitoring of lung mechanics, heart activity and lung perfusion and pulmonary function testing [35,36,38]. EIT has also been shown to be useful in the detection of pneumothorax [38].

Currently**,** CT and MRI scans are the most available technologies which achieve regional information on the lung. Those techniques provide snapshots of morphologic structures with high spatial resolution. In contrast, EIT has a poor spatial resolution but a very high temporal resolution [26]. Even though, the information of EIT and CT images appears similarities to each other by pathological conditions (e.g., pneumothorax), and most of the results of all experimental studies had suggested the tremendous potential clinical benefits of EIT when used for lung monitoring [38]. Yet, EIT had still not found a place in clinical practice, it can be just used as a complementary technique for daily used imaging modalities in hospitals.

In addition, the number of electrodes play an important role in EIT. A low number of electrodes (8 electrodes) will give an image with poor spatial resolution and few data points to reconstruct the image. On the other hand, when a higher number of electrodes (16 electrodes) is used, the spatial resolution of the tomography image will be improved, and more data points are obtained compared to a lower number of electrodes. However, a lower number of electrodes have also some advantages. It can be used for very small chest dimensions, for children and it will reduce also the EIT hardware productions costs.

In this thesis, we attempt to image the human chest using our developed EIT setup. 16 ECG electrodes were placed on the surface of the thorax by a 25 years-old man **(figure S1A)**. An AC current of 1 mA was injected (medical safe) and the boundary voltages were measured using the

adjacent method. The obtained boundary measurements were obtained, saved as TXT.file and post-processed using EIDORS library.

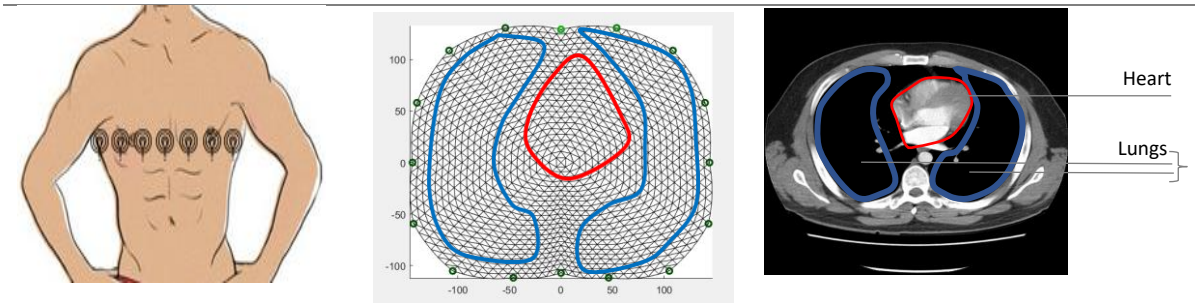

A: Apply currents and measure voltages on electrodes	**B**: Model where the data will be fitted to reconstruct the EIT image (FEM: Finite element model)	**C**: A CT-scan image of the lungs

Figure S1 A: *A schematic of the human body and how the electrodes are placed onto the surface of thorax.* ***B:*** *A 2D FEM model generated by EIDORS****. C:*** *A CT scan of the thorax.*

Figure S2 shows the obtained tomography images. The static (absolute) images show clearly two blue regions (less conductive), which are the lungs and one red region (more conductive) which is the heart muscle. Next, a clear difference can be observed between images with 8 electrodes and 16 electrodes, which means that the spatial resolution has been improved by increasing the number of electrodes.

EIT can also be used to measure the lung respiration since there is a difference between inspiration and expiration in lung volume. The resistivity of the lungs is influenced by inspiration as the alveoli swell and electrical current must flow around them. In our case, it was interested to make different images, but it was not possible due to the frame rate. The device setup (Agilent) needs approximately 14 minutes to make a full circle measurement. The tomography images are also influenced by the electrode positions and the body shape should be considered. Notice that this script is fitted in a thorax model. It uses a filter that give the expected results. However, this will not be considered as an algorithm to image the thorax.

In conclusion, all these results, make EIT a strong competitive candidate of the other conventional imaging techniques using this scrip in clinical research. But still, research and validation are needed.

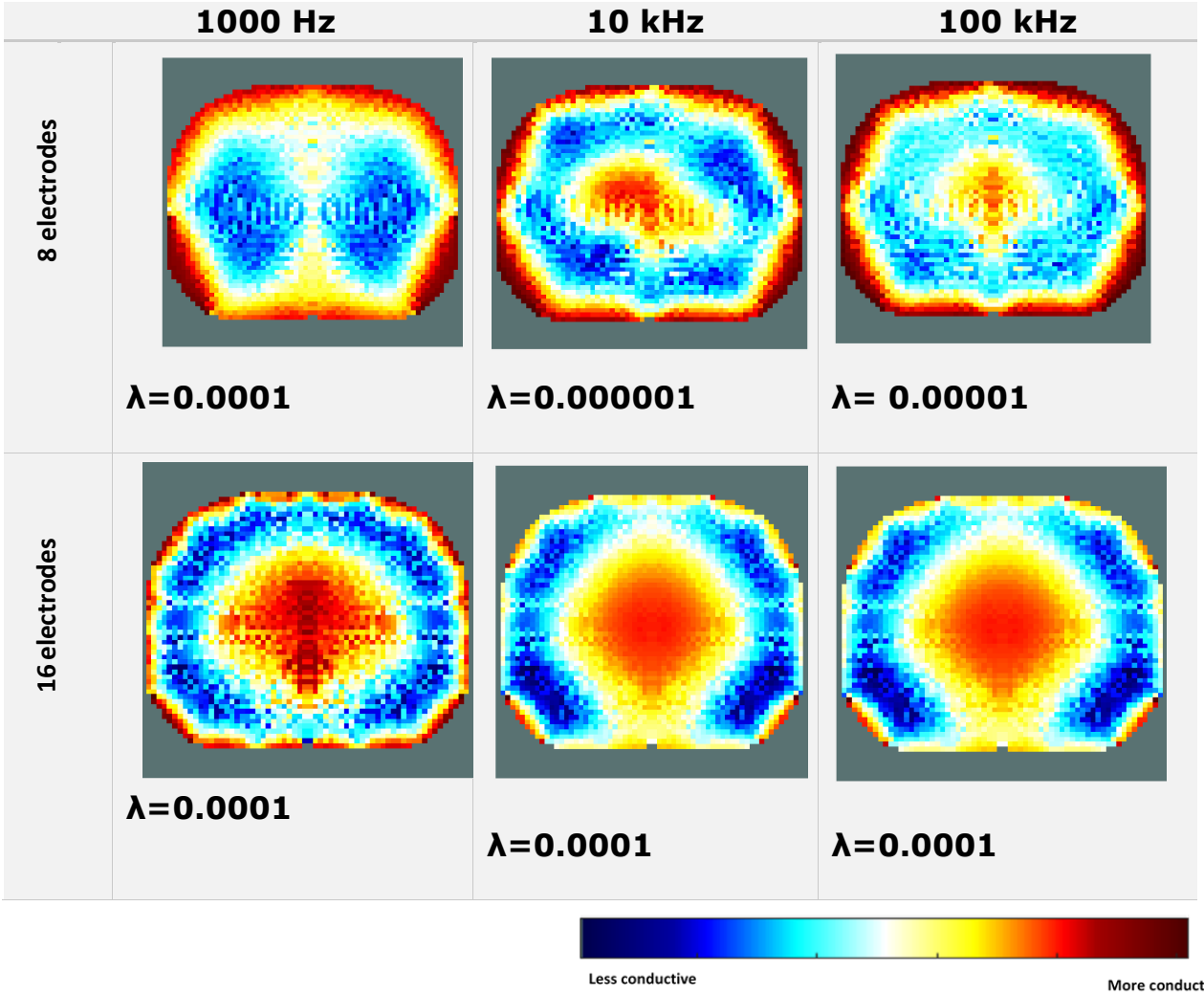

Figure S2 Static images of EIT using 8 electrodes and 16 electrodes*. The hyperparameter is manually chosen. The heart and the lungs can be observed clearly. However, this script uses a special filter and we should be carefully with it when we will use it in medical context.*

S1.2 EIT of the human bladder

One of the side purposes of this thesis is to image another human tissue, the bladder. EIT has been an interesting technique to determine the bladder volume and can be used to solve problems by patient groups who have defects in some neural structures which cause a damage of bladder volume sensation [39]. This often associated with the inability to urinate correctly. One of the used therapies in hospitals is a regular intermittent self-catheterization following a fixed time schedule. But, sometimes the interval of the emptying is not correctly chosen, too short or too long interval lead to some complications. A solution to this problem is thus a non-invasive continuous impedance-based volume monitoring of the bladder as have done by study Schlebusch et al. [39]. This system utilizes the difference in conductivity between urine and the tissue surrounding the bladder. Urine conductivity is mostly determined by its saline concentration and is usually in the impedance range of 5-26 mS/cm. In contrast, the tissues surrounding the bladder (muscles, fat, etc.) are in the impedance range of 0.2-4 mS/cm.

It was also interesting for to test our system by bringing the bladder in the image and to see if there is any difference in conductivity between a full bladder and an empty bladder. 16 ECG electrodes were placed at the level of the human bladder on a 25 years old man. The test person came with a full bladder (overnight urine volume), the measurements were performed and then on an empty bladder. A current of 10 mA, 20 mA, and 30 mA at different frequencies (1 kHz, 10 kHz) is injected to and the resulting voltage potential is measured using the adjacent method. The raw data was saved as TXT-file and post-processed using EIDORS library. The set-up is shown in **figure S3A.**

Absolute vs. difference imaging

As aforementioned, EIT seeks to calculate an image of the actual conductivity distribution within a body based on a single set of measurement. **Figure S5** shows a differential image; a simple abdominal geometry has been used and can be found in EIDORS. The data of a full bladder was subtracted from data of an empty bladder. The resulted image shows clearly the bladder region. The colour of this region is red which indicates the place of the bladder. Furthermore, the image is comparable with CT-scan **(figure S3C)**. The obtained results for the difference tomography measurements were comparable with CT scan of the abdomen. The bladder was clearly seen in the image.

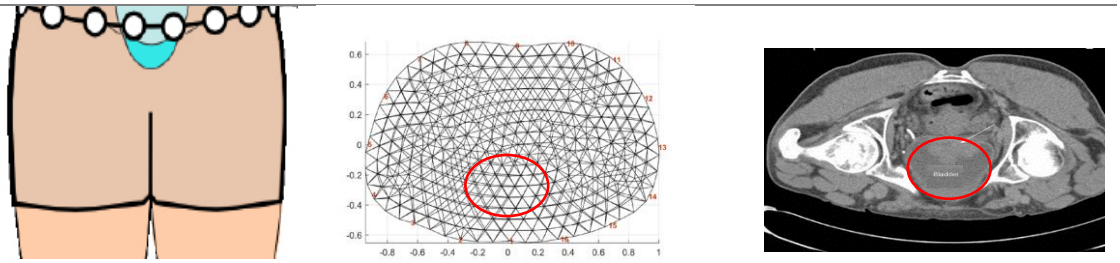

A: Apply currents and measure voltages on electrodes	**B**: Model where the data will be fitted to reconstruct an EIT image (FEM)	**C**: A CT-scan of the bladder region

***Figure S3 A**: A schematic of the human body and how the electrodes are placed on the surface of the thorax**. B**: A 2D FEM model generated by EIDORS. **C**: A CT scan of the thorax.*

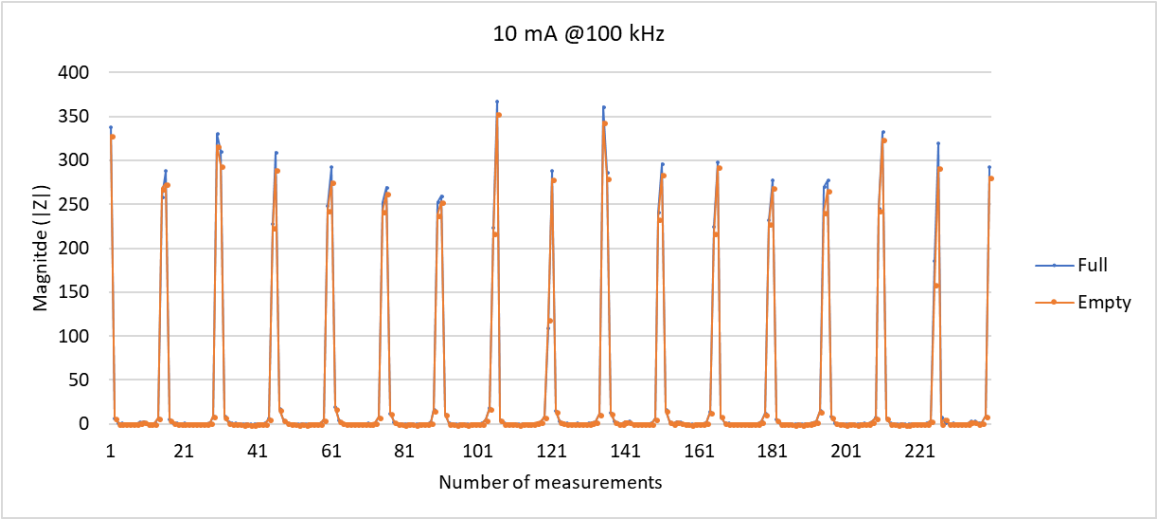

***Figure S4 Raw data of a full and empty bladder**. A full bladder shows a higher resistance.*

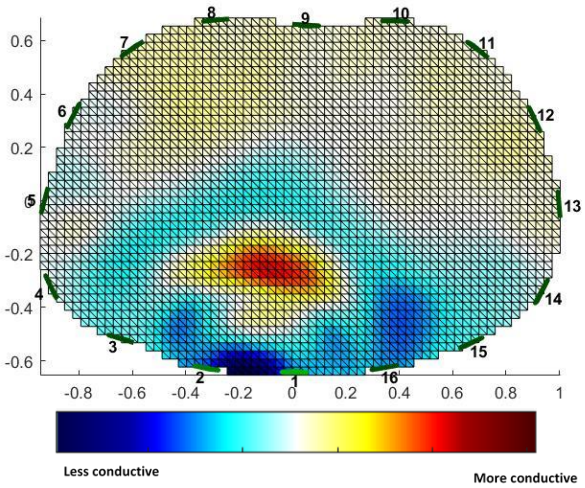

***Figure S5 Differential tomography image of the bladder.** The red region indicates the more conductive location, which is the bladder*. The image is comparable with CT-scan image.

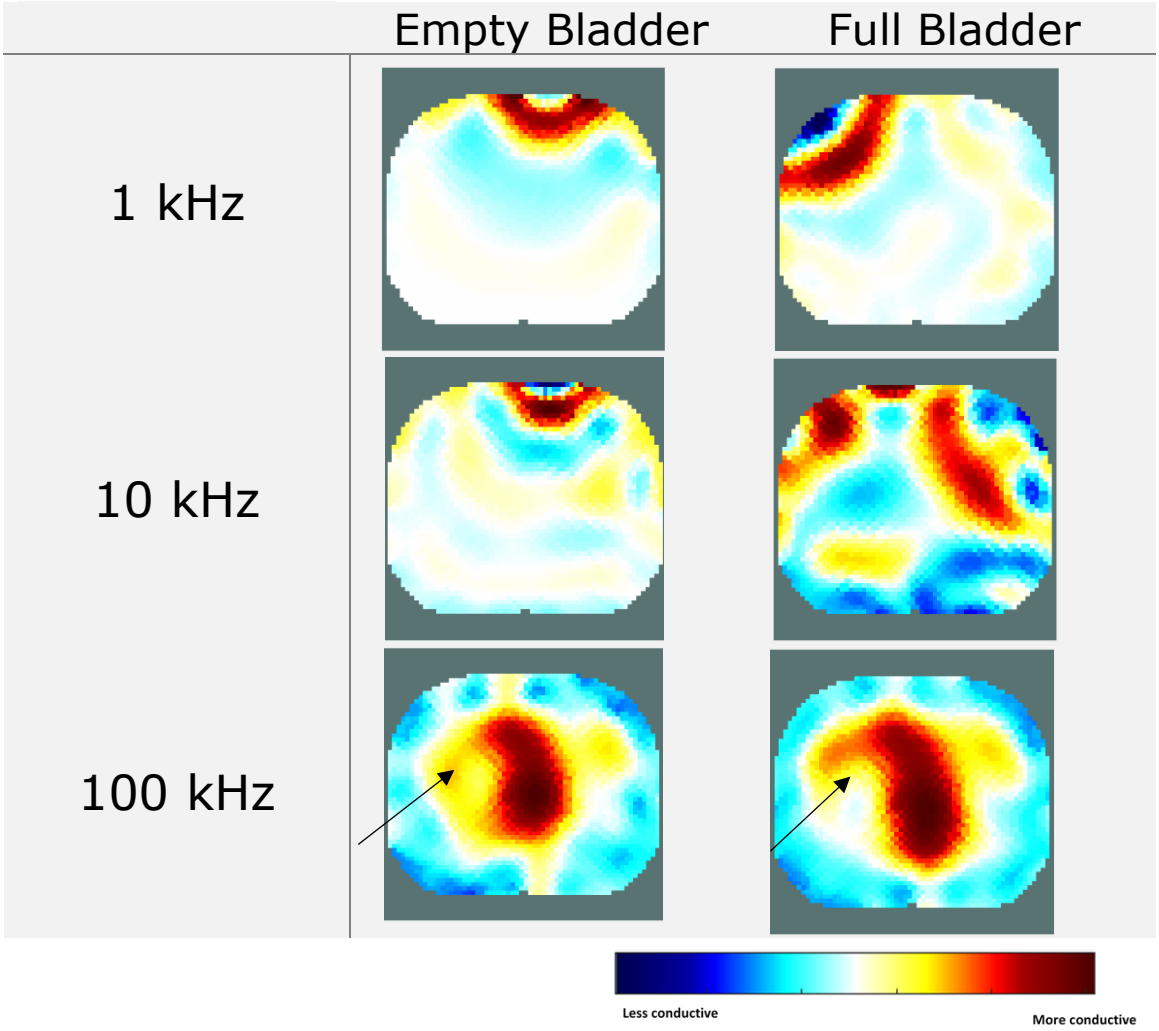

Figure S6 Reconstructed absolute images of a human bladder. *A clear difference in conductivity values can be observed between an empty bladder and a full bladder*. (*10 mA current at 100 kHz),*

The results illustrate a clear difference between a full bladder and an empty bladder in absolute images. Furthermore, the difference image shows clear similarities with a CT-Scan. The shape of the bladder is clearly seen in the tomography image. That indicates the powerful of the EIT technique. Still, further research is needed to use it in a patient's daily life.

S2 Flow chart of the internship IMO

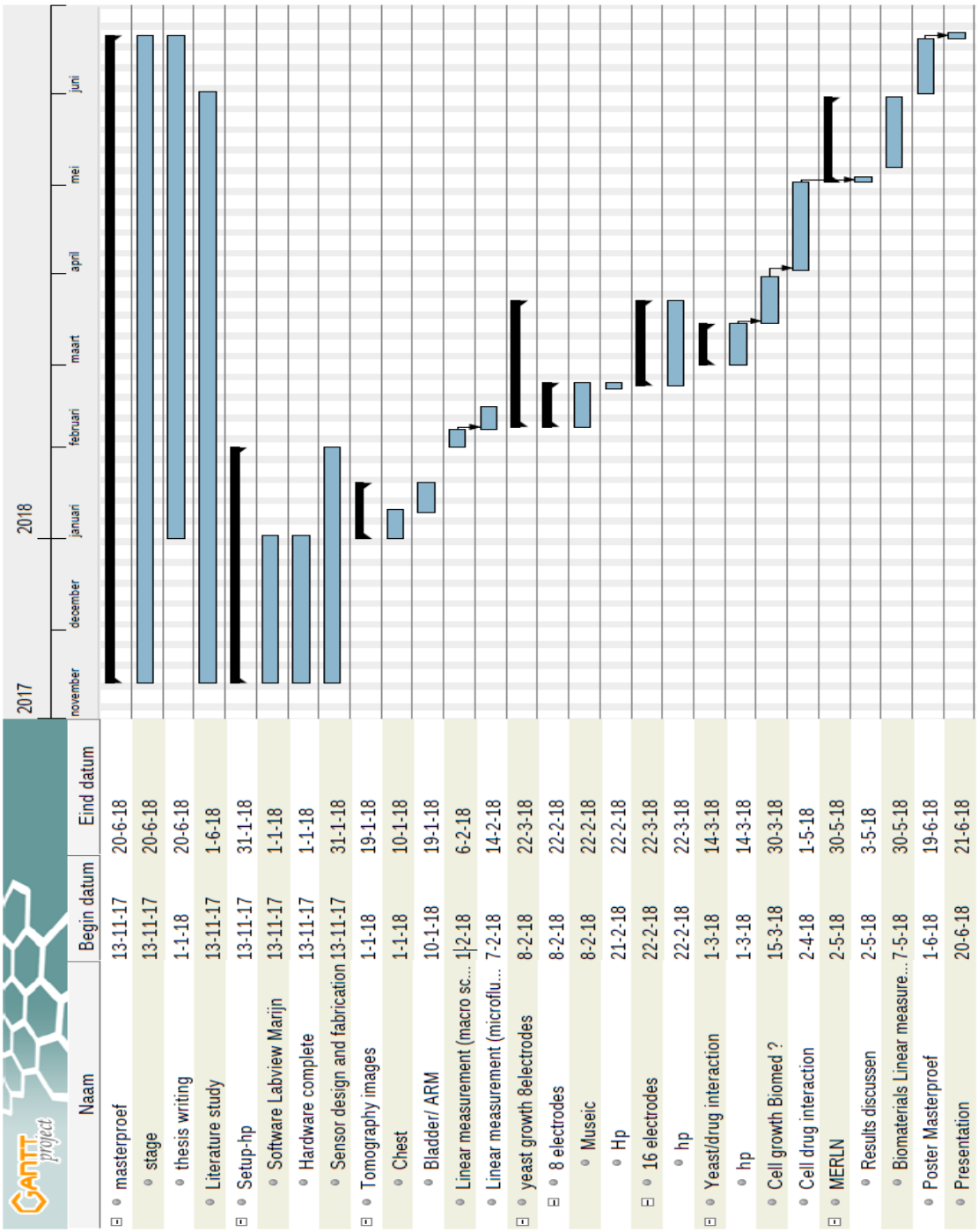

Naam	Begin datum	Eind datum
masterproef	13-11-17	20-6-18
stage	13-11-17	20-6-18
thesis writing	1-1-18	20-6-18
Literature study	13-11-17	1-6-18
Setup-hp	13-11-17	31-1-18
Software Labview Marijn	13-11-17	1-1-18
Hardware complete	13-11-17	1-1-18
Sensor design and fabrication	13-11-17	31-1-18
Tomography images	1-1-18	19-1-18
Chest	1-1-18	10-1-18
Bladder/ ARM	10-1-18	19-1-18
Linear measurement (macro sc...	1-2-18	6-2-18
Linear measurement (microflu...	7-2-18	14-2-18
yeast growth 8electrodes	8-2-18	22-3-18
8 electrodes	8-2-18	22-2-18
Museic	8-2-18	22-2-18
Hp	21-2-18	22-2-18
16 electrodes	22-2-18	22-3-18
hp	22-2-18	22-3-18
Yeast/drug interaction	1-3-18	14-3-18
hp	1-3-18	14-3-18
Cell growth Biomed ?	15-3-18	30-3-18
Cell drug interaction	2-4-18	1-5-18
MERLN	2-5-18	30-5-18
Results discussen	2-5-18	3-5-18
Biomaterials Linear measure...	7-5-18	30-5-18
Poster Masterproef	1-6-18	19-6-18
Presentation	20-6-18	21-6-18

Figure S7 Flow chart of the internship: unfortunately, the readout device gave some errors as result no tests were performed using animal cells.

S3 Extra information regarding this thesis

S3.1 The way of reconstruction EIT images

The tomography images in this thesis can be reconstructed using MATLAB script that we have used. The raw data and the script can be request it by the author or by the supervisor of this thesis. Furthermore, the parameters used are found in the following **table S1**.

Table S1 Shows the parameters of the way how the images are reconstructed using EIDORS library.

Figure	14	15	18	25	28	29	30
Solver	Gaussian-Newton	Gaussian-Newton	Gaussian-Newton	Gaussian-Newton	Gaussian-Newton	Gaussian-Newton	Gaussian-Newton
Prior	Laplace	Laplace	Laplace	Laplace	Laplace	Laplace	Laplace
Background	0.1 S/m	0.1 S/m	0.1 S/m	1 S/m	0.0004 S/m	1 S/m	1 S/m
Hyperparameter	0.002	0.00001	0.00001	0.000001	10 000	0.0001	0.00001
Normalized between (0-1)	Yes	Yes	Yes	Yes	Yes	Yes	Yes
Type of the image	Absolute	Differential	Absolute	Differential	Differential	Differential	Differential/ absolute
Current	1 mA	1 mA	100 μA	1 mA	10 mA	10 mA	5 mA
Method	Adjacent	Adjacent	Adjacent	Adjacent	Adjacent	Adjacent	Adjacent
Device	Agilent 4824A	Agilent 4824A	Agilent 4824A	Agilent 4824A	Agilent 4824A	Agilent 4824A	Agilent 4824A

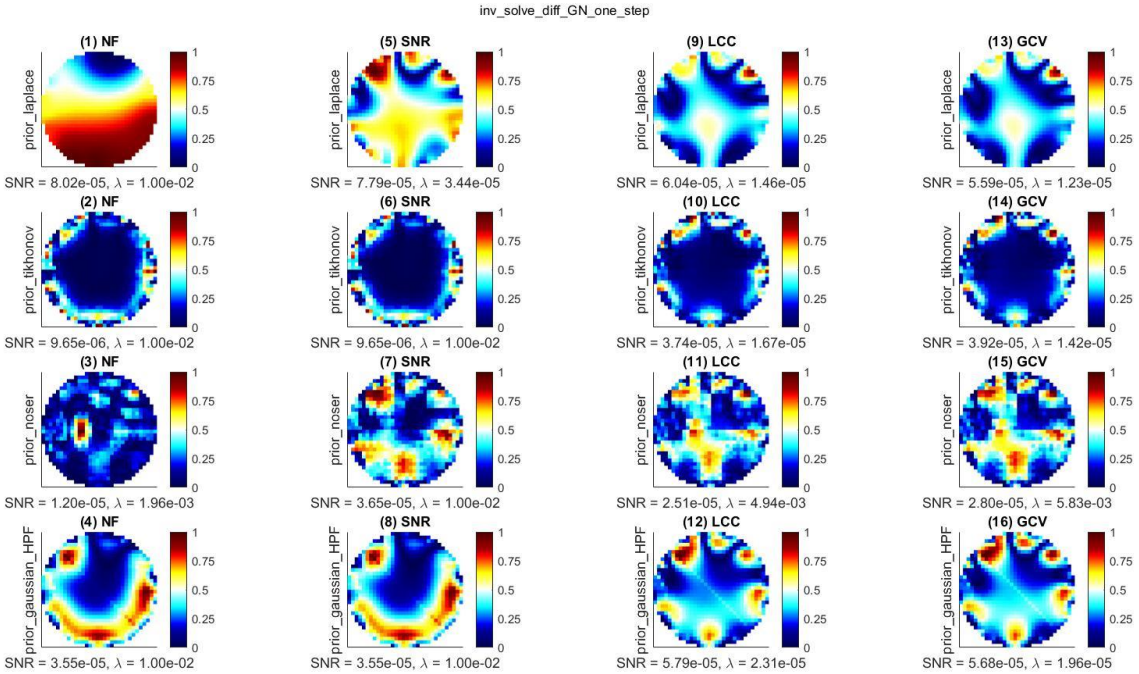

***Figure S8 Tomography images of a yeast grain on the top of the sensor using the combination script**. This last script allows us to get an idea about the best prior that can be chosen for the reconstruction of the images. Also, the hyperparameter is calculated in a such way that fits with the used data. However, that script uses heavy mathematical calculation and request some time to solve it. Notice that Laplace prior gave the most closed image to the reality, that is why we have use it for the whole images in this thesis.*

Auteursrechtelijke overeenkomst

Ik/wij verlenen het wereldwijde auteursrecht voor de ingediende eindverhandeling:
Electrical impedance tomography integrated with microfluidics: a characterization study for cell/tissue behaviour

Richting: **master in de biomedische wetenschappen-bio-elektronica en nanotechnologie**
Jaar: **2018**

in alle mogelijke mediaformaten, - bestaande en in de toekomst te ontwikkelen - , aan de Universiteit Hasselt.

Niet tegenstaand deze toekenning van het auteursrecht aan de Universiteit Hasselt behoud ik als auteur het recht om de eindverhandeling, - in zijn geheel of gedeeltelijk -, vrij te reproduceren, (her)publiceren of distribueren zonder de toelating te moeten verkrijgen van de Universiteit Hasselt.

Ik bevestig dat de eindverhandeling mijn origineel werk is, en dat ik het recht heb om de rechten te verlenen die in deze overeenkomst worden beschreven. Ik verklaar tevens dat de eindverhandeling, naar mijn weten, het auteursrecht van anderen niet overtreedt.

Ik verklaar tevens dat ik voor het materiaal in de eindverhandeling dat beschermd wordt door het auteursrecht, de nodige toelatingen heb verkregen zodat ik deze ook aan de Universiteit Hasselt kan overdragen en dat dit duidelijk in de tekst en inhoud van de eindverhandeling werd genotificeerd.

Universiteit Hasselt zal mij als auteur(s) van de eindverhandeling identificeren en zal geen wijzigingen aanbrengen aan de eindverhandeling, uitgezonderd deze toegelaten door deze overeenkomst.

Voor akkoord,

El Jerrari, Youssef

Datum: **7/06/2018**